Kinetic Analysis of Wired Enzyme Electrodes. Application to Horseradish Peroxidase Entrapped in a Redox Polymer Matrix

Juan Jose Calvente,*,† Arántzazu Narváez,‡ Elena Domínguez,‡ and Rafael Andreu*,†

Departamento de Química Física, Facultad de Química, Universidad de Sevilla, 41012-Sevilla, Spain, and Departamento de Química Analítica, Facultad de Farmacia, Universidad de Alcalá, 28871-Alcalá de Henares, Madrid, Spain

Received: January 8, 2003

A new approach to the description of the steady-state voltammetric behavior of wired enzyme electrodes in the presence of substrate mass transport polarization is presented. Starting from the exact analytical solutions corresponding to two-dimensional mediator−enzyme structures, experimental conditions are identified where the same equations can be applied to the analysis of the more often encountered three-dimensional catalytic films. These conditions are shown to involve a uniform redox conversion throughout the film. Case diagrams have been developed to assess the validity of this approach and to ascertain the influence of mass transport polarization and electron hopping on the voltammetric response. The relevance of the catalytic half-wave potential, as a direct measure of the ratio of the rates of redox mediation and enzyme turnover, is stressed. The kinetic analysis is applied to the electrocatalytic behavior of taurine-modified horseradish peroxidase, entrapped within a polyvinyl pyridine polymer containing osmium redox centers. This integrated electrochemical system is shown to be characterized by an efficient electronic connection between the catalytic and mediator centers, easy permeation of the substrate through the film, and a low value of the enzyme−substrate Michaelis constant. A sensitivity 20% higher than the maximum value previously reported in the literature for polymer-based peroxidase electrodes is obtained, and it appears to be related to a stronger electrostatic interaction between the negatively charged taurine modified HRP and the positively charged redox polymer. A comparison with kinetic parameters obtained in homogeneous solution (*J. Am. Chem. Soc.* **2002**, *124*, 240) suggests that further improvement of this electrode configuration would require a higher fraction of the immobilized enzymes to be effectively connected to the redox network.

Introduction

Enzyme electrodes have attracted considerable attention because of their ability to transduce a chemical event into an easy-to-use electrical signal.[1] Their strength relies on the high specificity of enzymes for recognizing target molecules and on an efficient renewal of the enzyme active form by means of an electrochemically driven redox reaction. Thus, the catalytic current measured in the presence of substrate can be used either to estimate the amount of a particular analyte or to gain new insights into the catalytic mechanism.

It is well-known that enzymatic redox sites are embedded into a protein matrix, making electron transfer rates prohibitively slow in most orientations. Nevertheless, direct electron transfer between electrodes and enzymes has been reported for small redox proteins, of 2×10^4 Da or less, with effective hydrodynamic radii of ∼21 Å.[1b,2] In search of an adequate electronic communication, strategic immobilization can provide the means to orientate the enzyme conveniently, thereby, achieving direct electron transfer through a selective pathway. Irrespective of the success of this approach, direct electron-transfer rates often remain low in comparison to turnover rates of the enzymes,[3] thereby, deteriorating the overall performance of the enzyme electrode.

Alternatively, mediated electron transfer, coupled to either diffusing or immobilized redox couples, can provide fast and efficient transduction schemes, though the presence of diffusing components should be avoided in those cases where a reagentless configuration is required. Several strategies have been developed to build fast electronic links between enzymes and electrodes. They include three basic approaches: (i) the tethering of redox relay groups to the protein providing a pathway for electron hopping,[4] (ii) the specific attachment of redox species to the electrode surface, most commonly by self-assembled heterofunctional monolayers,[5] and (iii) the deposition of bioelectrocatalytic films with either redox[6] or conducting[7] polymers, enabling electron exchange with the protein active center.

Irrespective of the electrode configuration, optimization of the biosensor performance requires a separate analysis of each bioelectrocatalytic step, including substrate reaction at the active enzyme site, electron transfer between enzyme and electrode, and substrate mass transport from the solution. An adequate modeling of the electrochemical behavior of these steps opens up the possibility to characterize the different processes that determine the sensor response, thus facilitating its rational design. In this context, Smyth et al.[8] have used the ratio between the turnover number and the Michaelis constant to assess the efficiency of organic phase enzyme electrodes. The boundary value problem associated with electrochemically driven catalyzed reactions is complex, because of the interplay of mass transport, charge propagation across the film, and nonlinear Michaelis−Menten kinetics.[9] In general, analytical solutions are not attainable, and two approaches have been adopted to cope with this problem: digital simulation and approximate analytical solutions for a number of limiting cases.[10]

Numerical solutions of the relevant diffusion-reaction equations have been reported by using different versions of the finite

* To whom correspondence should be addressed. Phone: +34-954557177. Fax: +34-954557174. E-mail: fonda. pacheco@us.es.
† Universidad de Sevilla.
‡ Universidad de Alcalá.

10.1021/jp030011p CCC: $25.00
Published on Web 06/12/2003

difference scheme[11] and the orthogonal collocation technique.[12] Both steady-state and transient responses have been worked out. However, most of the published material in this field deals with systems in which either the enzyme, or both enzyme and mediator, are free diffusing species, thus paying less attention to the case where enzyme and mediator are co-immobilized in an adsorbed film.

The approach based on the search of approximate analytical solutions was pioneered by Saveant et al.[13] and Albery and Hillman.[14] They reported a kinetic analysis of the reaction between a free diffusing substrate and a mediator bound to a polymer-modified electrode. Later incorporation of nonlinear enzyme kinetics resulted in a more involved mathematical problem, and approximate analytical solutions were derived for amperometric biosensors, by considering separately the cases of saturated and unsaturated kinetics.[15] More recently, Bartlett et al.[16] have developed a rather extensive approach, focusing on the diffusion-reaction coupling within a 3D biocatalytic film. They derived approximate analytical solutions for a number of limiting cases, whereas numerical solutions were obtained for intermediate situations.

The kinetic behavior of electrochemical biosensors is most commonly characterized from the dependence of the steady-state amperometric current on the substrate concentration. This type of analysis has some limitations because it does not allow for a decoupling of the enzyme−mediator and enzyme−substrate reaction rates. The additional information required to complete the kinetic analysis can be extracted either from the potential dependence of the steady-state catalytic current or from the shift of the half-wave potential with substrate concentration. Rotating disk voltammetry appears to be particularly well suited for analyzing the wave shape dependence on externally controlled parameters, such as substrate concentration or potential, because its mass transport conditions can be easily implemented within complex kinetic schemes. In a recent report, Savéant et al.[17] have presented the theoretical analysis of a closely related system, which includes an immobilized redox enzyme connected to the electrode by a freely diffusing mediator. They have discussed the shape of the transient and steady-state voltammetric waves in terms of the kinetic competition between substrate and cosubstrate and have also considered the influence of substrate diffusion on the current.

It is the aim of this work to describe the steady-state voltammetric behavior of a reagentless mediated enzyme electrode, taking into account the substrate depletion outside the biocatalytic film, and to illustrate its application to the case of the electrocatalytic behavior of taurine-modified horseradish peroxidase (HRP) entrapped within an osmium polymer gel.[3] Experimentally oriented zone diagrams and diagnostic criteria to assess the influence of diffusional effects, originated either in the substrate mass transport or in the charge propagation through the film, are also derived. The results reveal a good electrical connection between HRP and osmium redox centers, the need to account for substrate mass transport effects in the unsaturated kinetic region, and the control of the overall catalytic rate by the conversion of the HRP−H_2O_2 precursor complex into HRP−I and H_2O, in the saturated kinetic regime.

Experimental Section

Hydrogen peroxide (30%) was purchased from Merck. 2-Bromoethylamine hydrobromide $Br(CH_2)_2NH_2 \cdot HBr$ and Taurine (99%) were obtained from Aldrich. Poly(ethylene glycol 400 diglycidyl ether), technical grade (PEGDGE), was purchased from Polyscience. The redox polymer was synthesized by partial quaternisation of poly(vinylpyridine)$Os(bpy)_2Cl$ with 2-bromoethylamine hydrobromide as described in the literature.[18]

Horseradish peroxidase (HRP) EC 1.11.1.7. Type VI, from Sigma, was modified by oxidation of the glycosidic residues in order to render an overall negative charge after Schiff base formation with taurine.[6f] Briefly, 5 mg of native HRP were dissolved in 1 mL of 0.01 M carbonate buffer pH 9.5, and then 100 μL of 1% 2,4-dinitrobenzene dissolved in ethanol were added to protect the amino groups of the enzyme. The enzyme was activated by addition of 1 mL of a 0.08 M sodium periodate aqueous solution, and after 30 min of rotation in the dark, a 0.6 M ethylene glycol solution was added to stop the reaction. The solution was ultrafiltrated, extensively washed with carbonate buffer and collected in 2 mL of 0.1 M phosphate buffer pH 7, to which was added taurine powder to a 0.1 M final concentration. The reaction mixture was rotated during 3 h to form the Schiff base between the amino groups of taurine and the carbonyl groups of activated HRP. After reduction with a basic 30 mM $NaBH_4$ solution, the modified enzyme containing covalently bound sulfonate groups was purified by ultrafiltration, freeze-dried and stored at −18 °C until use. All other chemicals used were of analytical grade and used as received. The H_2O_2 solution was prepared daily.

All of the electrochemical measurements were performed in a conventional three electrode electrochemical cell using a computer controlled potentiostat Autolab/PGSTAT30. Potentials were measured against a potassium chloride-saturated silver/silver chloride electrode, whereas a Pt disk electrode served as counter electrode. The rotating electrode (AFE2M050AU) was a gold disk of 5 mm diameter, and it was operated by a AMSFRX analytical rotator from Pine. Prior to the enzyme immobilization, the gold RDE was polished successively with 0.3 and 0.05 μm alumina (Buehler) and finally sonicated in deionized water. A 0.1 M phosphate buffer solution at pH 7.0 was used as supporting electrolyte. Experiments were performed at 25 ± 0.5 °C.

To prepare the catalytic film, 1 μL of a 15 mg mL^{-1} modified HRP solution was mixed with 5 μL of a 12 mg mL^{-1} polymer solution, and 1 μL of this mixture was spread onto the clean gold surface. The electrodes were allowed to dry for 15 min, and 1 μL of a 1 mg mL^{-1} PEGDGE solution was then applied to promote cross-linking. The modified electrodes were cured at 28 °C in a water saturated atmosphere for 24−48 h before use.

Theory

(a) Two-Dimensional Model. Figure 1a shows a schematic representation of the model used to compute the electrochemical response of a rotating disk electrode, whose surface has been modified with an immobilized bioelectrocatalytic monolayer, including the enzyme of interest and a monoelectronic redox mediator couple. For the sake of generality, a double redox-enzyme catalytic cycle is considered.

Initially, in the presence of a large excess of substrate, only the oxidized forms of the mediator (O), enzyme (EO), and substrate (Z) exist. However, when a sufficiently negative electrode potential E is imposed, as in a voltammetric experiment, the following redox conversion takes place:

$$O + e^- \overset{E_s}{\rightleftharpoons} R \qquad (1)$$

where E_s is the standard potential of the redox mediator couple. Whenever newly formed R molecules face an oxidized enzyme

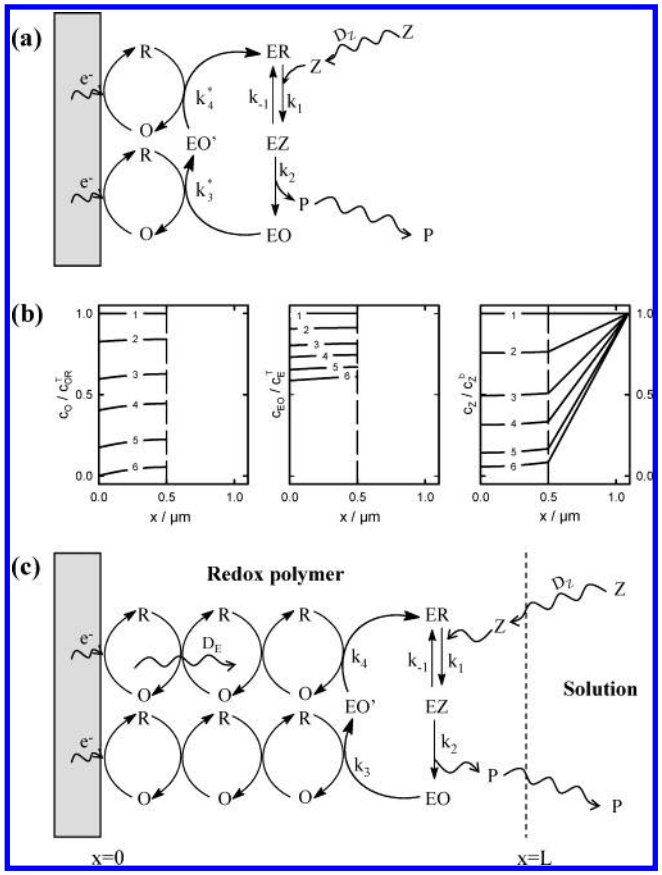

Figure 1. Schematic representation of a (a) bidimensional and (c) three-dimensional mediated enzyme electrode, subjected to a double redox-enzyme catalytic cycle, where R and O stand for the reduced and oxidazed forms of the redox mediator, ER for the native enzyme, EO and EO′ for the oxidized forms of the enzyme, Z for the substrate, and P for the product. (b) Normalized concentration profiles for O, EO, and Z as a function of the applied potential $E - E_s/V$: (1) 0.2, (2) 0.04, (3) 0.01, (4) −0.01, (5) −0.04, and (6) −0.2. Other parameter values: L = 0.5 μm, $c_E^T = 5 \times 10^{-8}$ mol cm^{-3}, $c_{OR}^T = 2 \times 10^{-4}$ mol cm^{-3}, $c_Z^b = 100$ μM, $D_Z = 8 \times 10^{-6}$ cm^2 s^{-1}, $D_E = 4 \times 10^{-9}$ cm^2 s^{-1}, $K_M = 1$ μM, $k_2 = 10^2$ s^{-1}, $k_3 = 3000$ M^{-1} s^{-1}, $k_4 = 10^9$ M^{-1} s^{-1}, and $\omega = 3000$ rpm.

molecule (EO), the following two step redox mediation reaction occurs:

$$R + EO \xrightarrow{k_3^*} O + EO' \quad (2a)$$

$$R + EO' \xrightarrow{k_4^*} O + ER \quad (2b)$$

where k_3^* and k_4^* are second-order surface rate constants, accounting for the rate of electron transfer between mediator molecules and the two oxidized forms of the enzyme EO and EO′, respectively. Then, the reduced form of the enzyme ER triggers the catalytic conversion of the substrate, according to the following Michaelis−Menten mechanism:

$$ER + Z \underset{k_{-1}}{\overset{k_1}{\rightleftharpoons}} EZ \quad (3a)$$

$$EZ \xrightarrow{k_2} EO + P \quad (3b)$$

Assuming a fast and reversible electron exchange between electrode and mediator and by adopting the steady-state hypothesis for the intermediate forms of the enzyme (see Appendix I), the following expression for the catalytic current corresponding to the previous reaction scheme is obtained:

$$i = \frac{FA\Gamma_{OR}^T}{1+\xi}\left(\mp\frac{\upsilon F}{RT}\frac{\xi}{1+\xi} - \frac{4k_3^{ap}\,\Gamma_E^T}{H+\sqrt{H^2-4G}}\right) \quad (4)$$

where the symbols have been defined in Appendix I. This expression describes the voltammetric wave as a superposition of a transient bell-shaped feature, associated with the redox conversion of the mediator (i_{rdx}), and a sigmoidal wave, originating from the catalytic conversion of the substrate (i_{cat}). The corresponding expression for the steady-state current measured at fixed potentials, i.e., by using the amperometric protocol, is easily derived by setting $\upsilon = 0$ in eq 4, and leaving the catalytic component unaffected.

A kinetic analysis based on eq 4 requires a nonlinear fitting procedure, due to the dependence of the catalytic component on the mass transport conditions. Nevertheless, particular experimental conditions can be envisaged where concentration polarization can be made negligible, and as a consequence, the kinetic analysis can be greatly simplified.

(a.1) Limiting Case in the Absence of Substrate Depletion. The extent of substrate depletion in the solution layer adjacent to the electrode is expected to depend on the ratio between the substrate flux required by the catalytic cycle and the flux supplied by the convection-diffusion transport rate. When the electrode rotation rate and the substrate bulk concentration are kept high enough, the required flux can be entirely supplied by mass transport without significant substrate depletion (i.e., $c_Z^s \approx c_Z^b$). This limiting case requires that the kinetic terms $k_2\,\Gamma_E^T$ (associated to the enzyme turnover) and $k_3^{ap}\Gamma_E^T\Gamma_{OR}^T$ (associated to the rate of electron exchange between enzyme and mediator) are much smaller than Λc_Z^b (associated to the mass transport rate), so that parameter H in Table AI.1 becomes independent of the hydrodynamic conditions, and adopts the following form:

$$H^* = 1 + \frac{k_3^{ap}\Gamma_{OR}^T}{k_2\,(1+\xi)}\left\{1 + \frac{K_M}{c_Z^b}\right\} \quad (5)$$

Moreover, G and U can be neglected against (H^*),[2] and the following expression for the voltammetric current is obtained:

$$i = \frac{FA\Gamma_{OR}^T}{(1+\xi)}\left\{\mp\frac{\upsilon F}{RT}\frac{\xi}{(1+\xi)} - \frac{2k_3^{ap}\,\Gamma_E^T}{1+\dfrac{k_3^{ap}\Gamma_{OR}^T}{k_2(1+\xi)}\left(1+\dfrac{K_M}{c_Z^b}\right)}\right\} \quad (6)$$

which also provides the steady-state amperometric response by setting $\upsilon = 0$.

An expression for the voltammetric limiting current i_L can be easily derived from eq 6 by noting that the i_L value is reached when $\xi \ll 1$ (i.e., when $E - E_s \to -\infty$), so that

$$i_L = \frac{-2FAk_3^{ap}\Gamma_{OR}^T\Gamma_E^T}{1+\dfrac{k_3^{ap}\Gamma_{OR}^T}{k_2}\left(1+\dfrac{K_M}{c_Z^b}\right)} \quad (7)$$

It is instructive to compare this expression with eq 7 in ref 17, which describes the limiting current in the case of a freely diffusing mediator, acting as a cosubstrate. In both cases, i_L equals the ratio between the maximum current that can be

supplied by the mediation step and $1 + \zeta$, where ζ is a dimensionless parameter accounting for the kinetic competition between substrate and mediator, either free diffusing or immobilized. This kinetic competition is described in the case of an immobilized mediator by

$$\zeta = \frac{k_3^{ap}\Gamma_{OR}^T}{k_2}\left(1 + \frac{K_M}{c_Z^b}\right) \tag{8}$$

Another useful experimental parameter, which is usually overlooked, is the half-wave potential of the catalytic current $E_{1/2}$. An expression for $E_{1/2}$ can be derived from the definition $i(E_{1/2}) = i_L/2$ and from eqs 6 and 7, to obtain

$$E_{1/2} = E_s + \frac{RT}{F}\ln(1 + \zeta) \tag{9}$$

According to eqs 7−9, i_L and $E_{1/2}$ of a given voltammogram are related by

$$i_L \exp\left\{\frac{F}{RT}(E_{1/2} - E_s)\right\} = -2FAk_3^{ap}\Gamma_{OR}^T\Gamma_E^T \tag{10}$$

where the right-hand side represents the maximum current that can be supplied by the mediation steps.

This relationship opens the possibility of determining the kinetic parameters in a sequential way. Thus, eq 10 provides the value of $k_3^{ap}\,\Gamma_{OR}^T\,\Gamma_E^T$, which can then be introduced into either eq 7 or eq 9 to estimate $k_2\Gamma_E^T$ under saturated kinetic conditions (i.e., when $c_Z^b \gg K_M$ and i_L becomes independent of c_Z^b). Knowing these two parameters, one can then use the dependence of the limiting current (eq 7), or of the half-wave potential (eq 9), on the substrate bulk concentration to determine the Michaelis constant. However, this last step should be performed with some caution, since the condition $c_Z^s \approx c_Z^b$ is expected to fail in the presence of low substrate bulk concentrations.

(b) Reduction of the 3D Kinetic Scheme to Its 2D Counterpart. To improve the sensitivity of the catalytic response, it is desirable to increase the number of enzyme molecules which are electrically wired to the electrode surface. Because of molecular packing restrictions, this increase results in the formation of 3D thin layer structures with typical thickness in the order of microns, where enzymes and redox mediators are closely intertwined. Figure 1c shows a schematic representation of this type of thin layer structure, formed by deposition of a redox gel with embedded enzyme molecules on the electrode surface.

As compared to the 2D scheme considered before, the 3D case involves the presence of two additional transport processes: substrate diffusion and electron hopping across the adsorbed layer of thickness L. In both cases, the transport is modeled as a diffusion process, whose characteristic parameters are the substrate diffusion coefficient D_Z and an apparent diffusion coefficient for the electronic charge propagation D_E, respectively. The corresponding boundary value problem, assuming steady-state conditions for the catalytic cycle, and a substrate partition coefficient between the film and the solution equal to one, is described in Appendix II. Different limiting cases, for which approximate analytical solutions are attainable, have been discussed in the literature.[16] Here, we will focus on the analytical solution in a situation where neither electron hopping nor diffusion of the substrate within the film determine the catalytic response. As compared to previous theoretical analysis of this type of electrochemical systems, we will include the possibility of substrate depletion in the solution layer adjacent to the film and will take advantage of the physical similarities with the 2D system described before.

Whenever the characteristic time scale of the slower diffusional process within the film (L^2/D_i, i = Z or E) is much smaller than the time scales of both the voltammetric potential scan ($RT/F\nu$) and the regeneration of the mediator oxidized form ($1/k_3^{ap}\Gamma_E^T$), uniform concentration profiles of the immobilized species and substrate are predicted throughout the film (Figure 1b). Under these circumstances, the 3D thin layer structure is expected to behave like the 2D structure described before. This situation is entirely analogous to that found in classical thin layer electrochemistry, with the exception that in the present case the film is facing a steady-state flux of substrate from the bulk of the solution. As in the case of classical thin layer protocols, the mathematical solution can be obtained from that of its surface analogue by an adequate reformulation of the characteristic variables.

For a uniform redox conversion across the film, the surface concentrations of any immobilized species Γ_i is given by

$$\Gamma_i = \int_0^L c_i(x)\,dx = c_i L \tag{11}$$

where c_i is the volume concentration of the species i within the film, which is assumed to depend on time, but not on the distance to the electrode surface x. Moreover, the substrate concentration within the film equals to its value at the film/solution interface c_Z^s

$$c_Z(x) = c_Z^s \tag{12}$$

This c_Z^s value can be obtained from the material balance of substrate within the film

$$\frac{dc_Z^s}{dt} = \frac{j_Z A}{V} - k_1 c_Z^s\frac{\Gamma_{ER}}{L} + k_{-1}\frac{\Gamma_{EZ}}{L} \tag{13}$$

where $V = LA$ is the volume of the film and j_Z is the flux of substrate entering the film at the film/solution interface, as defined by eq AI.14. Under steady-state conditions $dc_Z^s/dt = 0$, and eq 13 leads to an expression for c_Z^s which is identical to eq AI.16, derived for the 2D structure.

By substituting eq 11 into eqs AII.16−AII.19, the resulting expressions for Γ_{EO}, Γ_{EZ}, Γ_{ER}, and $\Gamma_{EO'}$ are again the same as those derived for the two-dimensional case, provided that k_3^s and k_4^s are reformulated as

$$k_3^s = k_3\,L^{-1} \quad \text{and} \quad k_4^s = k_4\,L^{-1} \tag{14}$$

where k_3 and k_4 are the rate constants for the homogeneous mediation process within the film (see Figure 1c).

This mathematical equivalence shows that the catalytic response of a 3D thin film, undergoing uniform redox conversion, approaches that of a 2D monolayer. Therefore, eqs 4 and 6−10 can be applied directly to the kinetic analysis of voltammetric waves associated with 3D films, provided that the time scale restrictions indicated above hold in a given experiment.

The equivalence between the 2D and the 3D approaches was further checked by comparing numerical voltammograms, corresponding to the general 3D kinetic problem described in Appendix II, with those derived analytically from eqs 4 and 6, and quantitative agreement was found in all cases. Diagnostic

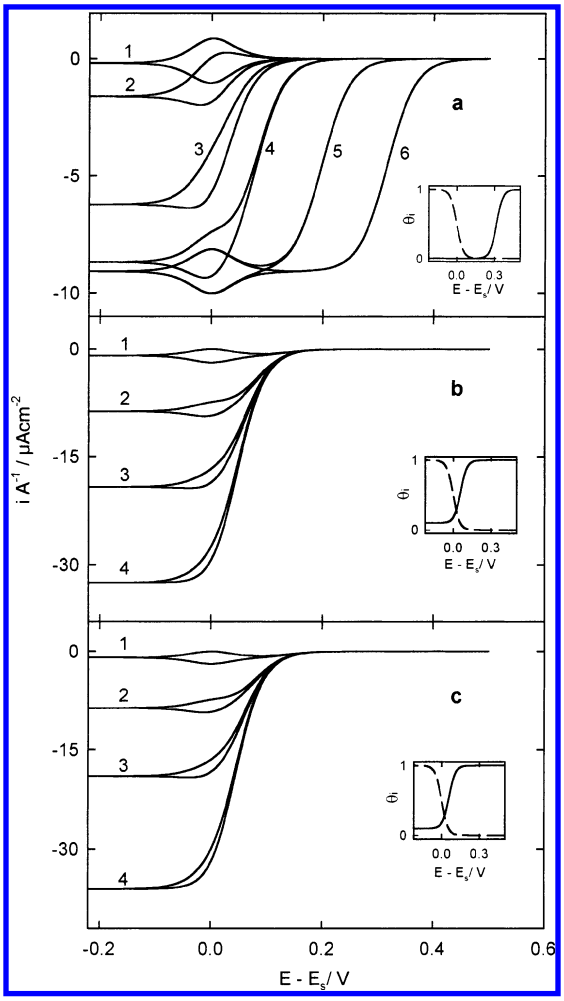

Figure 2. Influence of the kinetic parameters k_3^{ap}, k_2, and K_M on the voltammetric features of a two-dimensional enzyme electrode. (a) k_3^{ap}/mol^{-1} cm^2 s^{-1}: (1) 10^9, (2) 10^{10}, (3) 10^{11}, (4) 10^{12}, (5) 10^{14}, and (6) 10^{16}, $k_2 = 10^3$ s^{-1}, $K_M = 0.01$ M; (b) k_2/s^{-1}: (1) 10^2, (2) 10^3, (3) 2.5×10^3, (4) 5×10^3, $K_M = 0.01$ M, $k_3^{ap} = 10^{12}$ mol^{-1} cm^2 s^{-1}; and (c) K_M/M: (1) 0.1, (2) 0.01, (3) 4×10^{-3}, (4) 1.7×10^{-3}, $k_2 = 10^3$ s^{-1}, $k_3^{ap} = 10^{12}$ mol^{-1} cm^2 s^{-1}. Other parameter values: $\Gamma_E^T = 5 \times 10^{-12}$ mol cm^{-2}, $\Gamma_{OR}^T = 2\ 10^{-10}$ mol cm^{-2}, $c_Z^b = 100\ \mu$M, $D_Z = 8 \times 10^{-6}$ cm^2 s^{-1}, $E_s = 0$, and $\omega = 3000$ rpm. Insets show the potential dependence of the surface coverage ($\theta_i = \Gamma_i/\Gamma_i^T$) of species R (dashed lines) and EO (solid lines) for voltammograms (a) 6, (b) 3, and (c) 3.

criteria for the applicability of these simplified expressions will be discussed below.

Results and Discussion

(a) Voltammetric Shapes. As stated before, eq 4 leads to voltammetric waves that can be viewed as a superposition of a bell-shaped surface redox feature and a sigmoidal catalytic wave, though the overall appearance of the voltammogram depends on the actual values of the kinetic parameters (Figure 2).

For low values of the mediation rate constant k_3^{ap}, the catalytic wave develops at potentials close to the standard potential of the mediator couple, and the surface redox process shows up as an hysteresis loop of the current (see Figure 2a). This kind of hysteresis is often found in the literature, and according to the present model, it is brought about by the sign inversion of the surface redox component of the current i_{rdx} upon reversing the potential scan direction. As k_3^{ap} increases, the catalytic component shifts toward lower overpotential values, and eventually, it precedes the surface redox wave. The onset of the catalytic wave at such positive potentials reveals that only a tiny fraction of the surface bound mediator is required to sustain the catalytic cycle. In fact, this type of behavior had been anticipated experimentally by Heller et al.[3]

Figure 2, parts b and c, illustrates the influence of the k_2 and K_M values on the voltammetric shape. As k_2 increases, or K_M decreases, the catalytic current is progressively enhanced and, simultaneously, the wave is slightly shifted toward the standard potential of the redox mediator. Because of the enhancement of the catalytic component, the presence of the hysteresis loop induced by the surface redox component is progressively less evident. It should be noted that voltammetric shapes provide only a qualitative indication of the joint influence of k_2 and K_M, because there appears to be no specific features associated with their individual values.

Kinetic information on these systems can be obtained from the analysis of the dependence of the limiting current (i_L) and half-wave potential ($E_{1/2}$) on substrate concentration. The influence of the k_2 and k_3^{ap} values on some typical i_L vs c_Z^b, and $E_{1/2} - E_s$ vs c_Z^b, plots is illustrated in Figures 3a−d. It is seen that i_L ($E_{1/2}$) increases (decreases) with c_Z^b until it reaches a saturation value i_L^{sat} ($E_{1/2}^{sat}$). Analytical expressions for i_L^{sat} and $E_{1/2}^{sat}$ can be obtained by imposing that $c_Z^b \gg K_M$ in eqs 7−9, so that

$$i_L^{sat} = \frac{-2FAk_3^{ap}\Gamma_{OR}^T\Gamma_E^T}{1 + \dfrac{k_3^{ap}\Gamma_{OR}^T}{k_2}} \tag{15}$$

$$E_{1/2}^{sat} = E_s + \frac{RT}{F}\ln\left(1 + \frac{k_3^{ap}\Gamma_{OR}^T}{k_2}\right) \tag{16}$$

It should be noted that i_L increases with either k_2 or k_3^{ap}, whereas the half-wave potential displays a distinct behavior with respect to these two parameters (see Figure 3, parts b and d). An increase of k_2 shifts the wave toward the standard potential of the redox mediator, i.e., $E_{1/2} - E_s \to 0$ as $k_2 \to \infty$, whereas an increase of k_3^{ap} displaces the catalytic wave away from E_s, i.e., $E_{1/2} - E_s \to \infty$ as $k_3^{ap} \to \infty$, revealing that $E_{1/2} - E_s$ contains information on k_3^{ap} even when the redox mediation steps are not rate determining.

Figure 4 illustrates the influence of mass transport control on the i_L vs c_Z^b and $E_{1/2} - E_s$ vs c_Z^b plots. When $k_2\Gamma_E^T$ and $k_3^{ap}\Gamma_{OR}^T\Gamma_E^T$ are both bigger than the mass transport rate Λc_Z^b, substrate cannot be supplied at the rate demanded by the catalytic cycle (i.e., $c_Z^s < c_Z^b$), and the limiting current and half-wave potential become dependent on the electrode rotation speed. Now, the c_Z^b values required to reach the saturation behavior increase progressively as the rotation rate decreases. It should be noted that, for i_L values to become independent of c_Z^b, both conditions $c_Z^b \gg K_M$ and $c_Z^s \approx c_Z^b$ have to be met simultaneously. Once the saturation regime is reached, i_L^{sat} and $E_{1/2}^{sat}$ are not affected by the mass transport process. A more detailed analysis of the requirements for avoiding mass transport control is considered next.

(b) Applicability of the $c_Z^s \approx c_Z^b$ Limiting Case. Equations 6−9 provide a quantitative description of the catalytic wave for any value of the kinetic parameters k_2, k_3^{ap}, and K_M, in the absence of mass transport control. However, their applicability in a given experimental situation depends on the substrate bulk concentration, the electrode rotation speed, and the potential of interest along the catalytic wave. Figure 5a shows a comparison between the voltammetric behavior predicted by eq 4, which

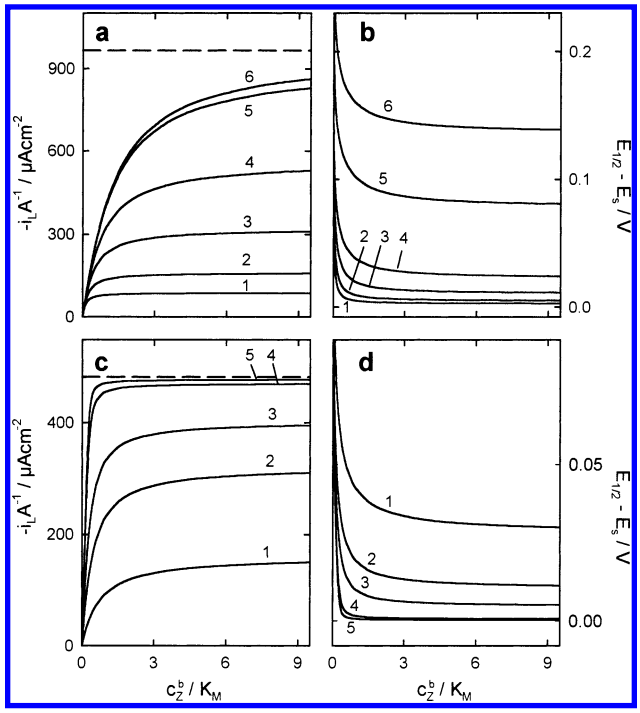

Figure 3. Dependence of the limiting current (a, c) and the half-wave potential (b, d) on the substrate bulk concentration, as a function of the kinetic parameters k_2 and k_3^{ap}. Upper panel (a,b): $k_2 = 1 \times 10^3$ s^{-1} and k_3^{ap}/mol^{-1} cm^2 s^{-1}: (1) 5×10^{11}, (2) 1×10^{12}, (3) 2.5×10^{12}, (4) 7×10^{12}, (5) 1×10^{14}, (6) 1×10^{15}. Lower panel (c,d): $k_3^{ap} = 2.5 \times 10^{12}$ mol^{-1} cm^2 s^{-1} and k_2/s^{-1}: (1) 2.5×10^2, (2) 1×10^3, (3) 2.5×10^3, (4) 2×10^4, (5) 5×10^4. Other parameter values: $K_M = 1$ mM, $\Gamma_E^T = 5 \times 10^{-12}$ mol cm^{-2}, $\Gamma_{OR}^T = 2 \times 10^{-10}$ mol cm^{-2}, $D_Z = 8 \times 10^{-6}$ cm^2 s^{-1}, $E_s = 0$, and $\omega = 3000$ rpm. Broken line in part a corresponds to $i_L A^{-1} = -2Fk_2\Gamma_E^T$. Broken line in part c corresponds to $i_L A^{-1} = -2Fk_3^{ap}\Gamma_{OR}^T\Gamma_{OR}^T$.

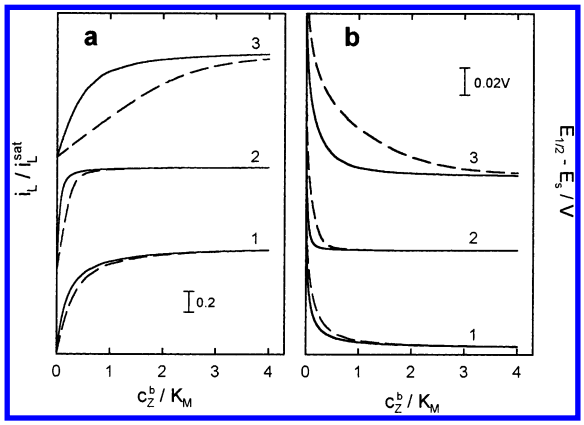

Figure 4. Influence of mass transport on the dependence of the normalized limiting current (a) and half-wave potential (b) on the substrate bulk concentration, as a function of the electrode rotation rate (3000 rpm solid lines and 100 rpm dashed lines) and the kinetic parameters values: (1) $k_2 = 5 \times 10^2$ s^{-1}, $k_3^{ap} = 5 \times 10^{11}$ mol^{-1} cm^2 s^{-1}, (2) $k_2 = 5 \times 10^3$ s^{-1}, $k_3^{ap} = 5 \times 10^{11}$ mol^{-1} cm^2 s^{-1}, (3) $k_2 = 5 \times 10^3$ s^{-1}, $k_3^{ap} = 5 \times 10^{12}$ mol^{-1} cm^2 s^{-1}. Other parameter values: $K_M = 1$ mM, $\Gamma_E^T = 5 \times 10^{-12}$ mol cm^{-2}, $\Gamma_{OR}^T = 2 \times 10^{-10}$ mol cm^{-2}, $D_Z = 8 \times 10^{-6}$ cm^2 s^{-1}, $E_s = 0$. For the sake of clarity plots 2 and 3 have been shifted upward.

incorporates mass transport effects, and by eq 6, which assumes $c_Z^s \approx c_Z^b$. Good coincidence along the whole voltammetric wave is obtained at high enough substrate concentrations (or high enough rotation rates, not shown), whereas significant deviations are observed in the presence of low substrate concentrations.

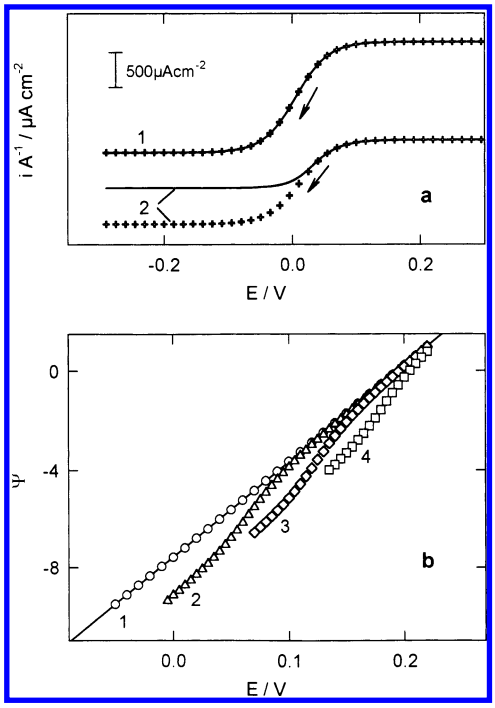

Figure 5. (a) Influence of substrate mass transport on a thin-layer enzyme voltammogram and (b) its assessment through the potential dependence of the Ψ function (see eq 22) for different substrate concentrations c_Z^b: (a) (1) 10 mM, (2) 500 μM, and (b) (1) 10 mM, (2) 100 μM, (3) 10 μM, (4) 1 μM. Symbols correspond to the $c_Z^s = c_Z^b$ limiting case (i.e., absence of mass transport effects). Other parameter values: $\Gamma_E^T = 5 \times 10^{-12}$ mol cm^{-2}, $\Gamma_{OR}^T = 2 \times 10^{-10}$ mol cm^{-2}, $D_Z = 8 \times 10^{-6}$ cm^2 s^{-1}, $E_s = 0$, $K_M = 1$ mM, $k_2 = 1 \times 10^4$ s^{-1}, $k_3^{ap} = 1 \times 10^{13}$ mol^{-1} cm^2 s^{-1}, and $\omega = 3000$ rpm.

To identify the potential range where the $c_Z^s \approx c_Z^b$ approximation holds, a useful experimental criterion can be derived from the potential dependence of i_{cat}. Thus, it follows from eqs 6 and 7 that

$$\Psi \equiv \ln\left(\frac{1}{|i_{cat}|} - \frac{1}{|i_L|}\right) = -\ln(2FAk_3^{ap}\Gamma_{OR}^T\Gamma_E^T) + \frac{F}{RT}(E - E_s) \tag{17}$$

and a plot of Ψ vs $E - E_s$ should be linear with a slope equal to F/RT. Figure 5b illustrates how the potential range where eq 17 is obeyed, and the $c_Z^s \approx c_Z^b$ approximation holds, is progressively reduced to the foot of the wave upon decreasing c_Z^b.

To assess the validity of the $c_Z^s \approx c_Z^b$ approximation for the entire catalytic wave, a case diagram can be constructed in terms of the following dimensionless parameters:

$$\rho_1 = \frac{k_2\Gamma_E^T}{\Lambda c_Z^b\left(1 + \dfrac{K_M}{c_Z^b}\right)} \tag{18}$$

$$\rho_2 = \frac{k_3^{ap}\Gamma_E^T\Gamma_{OR}^T}{\Lambda c_Z^b} \tag{19}$$

where each parameter represents the ratio between the flux required by either enzyme/substrate or enzyme/mediator kinetics and the flux supplied by mass transport. Case diagrams computed for several K_M/c_Z^b values are depicted in Figure 6. Solid lines were drawn in the ln ρ_1, ln ρ_2 plane corresponding to a difference of less than 1% between the i_L values obtained

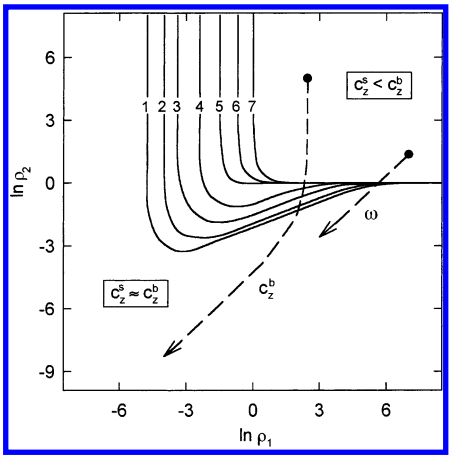

Figure 6. Zone diagram for the applicability of the $c_Z^s \approx c_Z^b$ limiting case in the analysis of the electrocatalytic response of a thin-layer enzyme electrode, as a function of the K_M/c_Z^b ratio: (1) ≥10, (2) 1.0, (3) 0.3, (4) 0.1, (5) 0.03, (6) 0.01, and (7) $\leq 1 \times 10^{-3}$. Arrow-ended dashed lines show the trajectories associated with an increase of either the substrate bulk concentration c_Z^b or the electrode rotation rate ω.

from eqs 4 and 6 and, therefore, indicate the applicability limits for the $c_Z^s \approx c_Z^b$ approximation. The zone diagrams reveal that this approximation is valid whenever ln $\rho_1 < -5$, or ln $\rho_2 < -3$. However, less stringent conditions are required as the K_M/c_Z^b ratio decreases; thus, it suffices that either ln $\rho_1 < 0$, or ln $\rho_2 < 0$, when $K_M/c_Z^b < 10^{-3}$. For a given electrode assembly, the electrochemical response can be brought into the $c_Z^s = c_Z^b$ zone by increasing either the substrate concentration or the electrode rotation rate, as illustrated in Figure 6 for two typical trajectories. It should be noted that, to displace the electrochemical system along the zone diagram, it is more effective to modify the substrate concentration than the rotation rate, due to the square root dependence of Λ on ω.

(c) Kinetic Analysis. Before attempting a kinetic analysis of the catalytic process, it is convenient to perform a voltammetric characterization of the enzyme-mediator film in the absence of substrate. Values of E_s and Γ_{OR}^T can be obtained from the peak potentials and the integration of the voltammetric wave, respectively, whereas the determination of Γ_E^T usually requires independent nonelectrochemical measurements. It should be noted that the catalytic rate also reflects the adequacy of the spatial connections between the biosensor components, and lower values of $k_3^{ap}\Gamma_{OR}^T\Gamma_E^T$ or $k_2\Gamma_E^T$ are to be expected whenever only a fraction of the redox centers, or of the immobilized enzymes, are effectively involved in the catalytic cycle.

Close inspection of eq 4 and Table AI.1 reveals that only three groups of parameters, i.e., $k_3^{ap}\Gamma_{OR}^T/k_2$, $k_2\Gamma_E{}^T/\Lambda$, and K_M, can univocally be determined from i_{cat} values recorded as a function of substrate concentration, electrode potential, and rotation speed. An adequate choice of the experimental conditions allows for a consistent decoupling of the kinetic parameters. This choice is largely determined by the possibility of attaining saturated and nonsaturated kinetic conditions in the absence of mass transport limitations, as shown next.

(c.1) Absence of Substrate Concentration Gradients. Analytical expressions derived for the $c_Z^s \approx c_Z^b$ limiting case provide a straightforward route to perform the kinetic analysis in a sequential way. This limiting behavior is more likely to be found for high values of c_Z^b and ω, and it can be confirmed through a Ψ vs $E - E_s$ plot (see eq 17 and Figure 5b). Then, $k_3^{ap}\Gamma_{OR}^T\Gamma_E^T$ can be obtained either from the plot intercept, or from eq 10. This $k_3^{ap}\Gamma_{OR}^T\Gamma_E^T$ value can be inserted in eqs 15 or 16 to determine $k_2\Gamma_E^T$, as long as $k_2\Gamma_E^T$ is not much larger than $k_3^{ap}\Gamma_{OR}^T\Gamma_E^T$. Therefore, the value of $k_2\Gamma_E^T$ becomes available only when $E_{1/2}^{sat} > E_s$, i.e., when the catalytic wave develops at potentials more positive than E_s. In the absence of mass transport control, the kinetic analysis can be concluded by determining K_M (or $K_M/k_2\Gamma_E^T$, if $k_2\Gamma_E^T$ is not attainable) from the variation of either i_L or $E_{1/2}$ with c_Z^b under nonsaturated conditions (see eqs 7−9).

Savéant et al.[20] and Calvo et al.[6d] have analyzed the catalytic oxidation of glucose by glucose oxidase immobilized on an electrode surface in terms of an expression analogous to eq 6 with $\upsilon = 0$. The kinetic analysis of Savéant et al.[20] involves two steps, first $k_3^{ap}\Gamma_{OR}^T\Gamma_E^T$ is obtained from the slope of a i_{cat}^{-1} vs $1 + \xi$ plot (primary plot), then the intercepts of the primary plots are plotted vs $1/c_Z^b$ (secondary plots) to derive the values of $k_2\Gamma_E^T$ and K_M. On the other hand, the kinetic analysis of Calvo et al.[6d] combines the use of the primary plots with a nonlinear fit of the i_L dependence on c_Z^b. As compared to these two approaches, the kinetic protocol outlined above avoids nonlinear fitting or extrapolation procedures.

(c.2) Absence of Substrate Concentration Gradients in the Saturated Kinetic Regime Only. Because of mass transport limitations at low substrate concentrations, a full analysis of the i_L (or $E_{1/2}$) vs c_Z^b plots is expected to require the use of the more general eq 4. Assuming that $k_3^{ap}\Gamma_{OR}^T\Gamma_E^T$ and $k_2\Gamma_E^T$ can still be obtained in the saturated kinetic regime as outlined above, the remaining parameters to be determined in the presence of lower substrate concentrations are the diffusion coefficient D_Z and the Michaelis constant K_M. In principle, both parameters can be estimated from a two-parameters fit of the variation of i_L with c_Z^b. However, it is found that, within experimental error, similar fits can be achieved for different pairs of D_Z, K_M values, and a more discriminating procedure is needed.

In the limit of very low substrate concentrations and negative enough potentials, the kinetic parameter H defined in Table AI.1 reduces to

$$(H_{\xi=0})_{c_Z^b \to 0} \approx \frac{k_3^{ap}\Gamma_{OR}^T\Gamma_E^T}{c_Z^b}\left(\frac{K_M}{k_2\Gamma_E{}^T} + \frac{1}{\Lambda}\right) \qquad (20)$$

and 4 $(G_{\xi=0})_{c_Z^b \to 0} \ll (H_{\xi=0})^2_{c_Z^b \to 0}$, so that the catalytic limiting current can be expressed as

$$(i_L)_{c_Z^b \to 0} = \frac{-2FAc_Z^b}{\dfrac{K_M}{k_2\Gamma_E^T} + \dfrac{1}{\Lambda}} = -\Phi c_Z^b \qquad (21)$$

The Φ/A ratio is often used to define the sensitivity of the biosensor, which may be seen to depend on its intrinsic properties (i.e., on the $K_M/k_2\Gamma_E^T$ ratio) in the $\Lambda \to \infty$ limit only. The rotation speed dependence of the initial slope Φ in a i_L vs c_Z^b plot can be used to obtain a first estimate of D_Z and K_M, as illustrated in Figure 7, parts a and b. A plot of Φ^{-1} vs $\omega^{-1/2}$ should be linear, and its slope and intercept provide the values of D_Z and $K_M/k_2\Gamma_E^T$, respectively. Then, more accurate values of these two parameters can be derived by an iterative procedure, which takes advantage of the distinct sensitivity of the i_L values toward D_Z and K_M under particular experimental conditions. Thus, starting with the previous D_Z estimate, an improved K_M value is obtained from a fit of the whole i_L vs c_Z^b plot, recorded at a high enough electrode rotation rate in order to reduce the influence of substrate mass transport (see Figure 7c). In a second iteration step, this K_M value is used to improve the estimate of

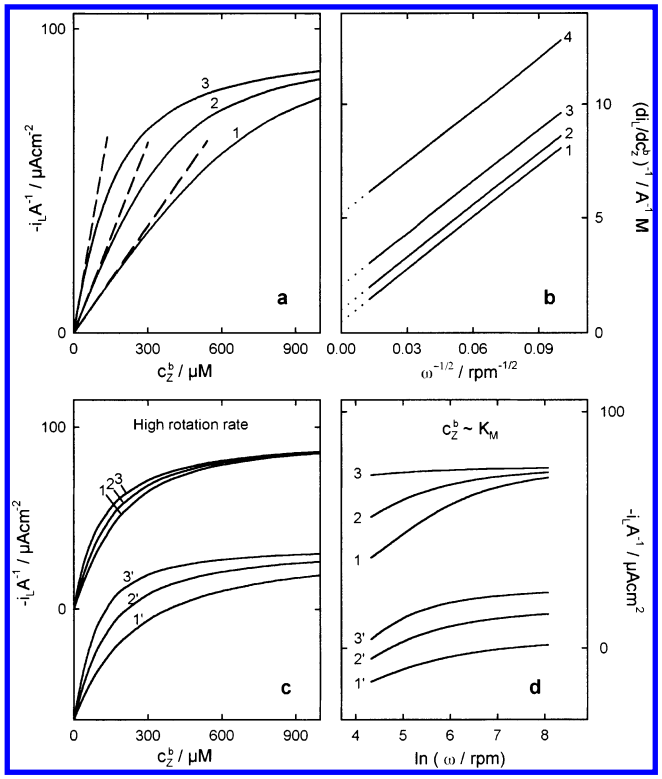

Figure 7. Upper panels (a,b): Illustration of the method used to obtain a first estimate of the D_z and K_M values. (a) Influence of the electrode rotation rate on the limiting current vs substrate concentration plots at (1) 100 rpm, (2) 400 rpm, and (3) 5000 rpm, with $K_M = 0.01$ M, $D_z = 2 \times 10^{-6}$ cm^2 s^{-1}. (b) The inverse of the limiting slopes in part a as a function of $\omega^{-1/2}$, with $D_z = 2 \times 10^{-6}$ cm^2 s^{-1} and K_M^{ap}: (1) 1000 s cm^{-1}, (2) 400 s cm^{-1}, (3) 200 s cm^{-1}, (4) 100 s cm^{-1}. Lower panels (c,d): Distinct sensitivity of the (c) $i_L A^{-1}$ vs c_Z^b and (d) $i_L A^{-1}$ vs ln(ω) plots toward D_z/cm^2 s^{-1}: (1) 2×10^{-6}, (2) 5×10^{-6}, (3) 5×10^{-5} and K_M/M: (1′) 0.02, (2′) 0.01, and (3′) 5×10^{-3}. For the sake of clarity, primed curves have been shifted downward. Plots in c were computed with $\omega = 3000$ rpm and $K_M = 0.01$ M. Plots in d were computed with $c_Z^b = 400$ μM and $D_z = 5 \times 10^{-6}$ cm^2 s^{-1}.Other parameter values: $\Gamma_E^T = 5 \times 10^{-12}$ mol cm^{-2}, $\Gamma_{OR}^T = 2 \times 10^{-10}$ mol cm^{-2}, $E_s = 0$, $k_2 = 10^4$ s^{-1}, and $k_3^{ap} = 10^{13}$ mol^{-1} cm^2 s^{-1}.

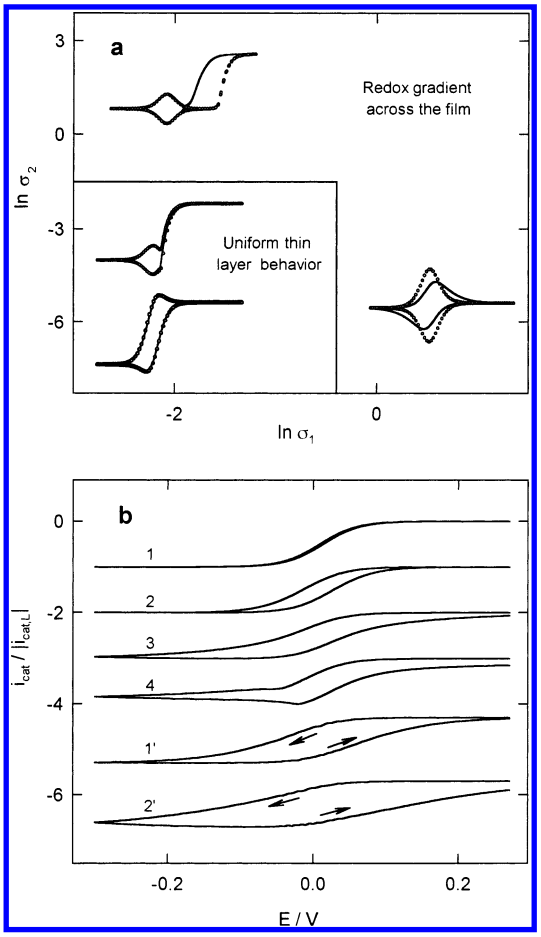

Figure 8. (a) Case diagram for the applicability of the uniform thin-layer model to characterize the voltammetric response of a reagentless enzyme electrode. (b) Influence of the film thickness L: (1) 0.5 μm, (2) 2.0 μm, (3) 5.0 μm, (4) 10.5 μm, with $v = 5$ mV s^{-1}, and of the scan rate v: (1′) 50 mV s^{-1}, (2′) 300 mV s^{-1}, with L = 1.0 μm, on the shape of the i/i_L normalized catalytic voltammograms. Other parameter values: $c_E^T = 5 \times 10^{-8}$ mol cm^{-3}, $c_{OR}^T = 2 \times 10^{-4}$ mol cm^{-3}, $c_Z^b = 500$ μM, $D_Z = 8 \times 10^{-6}$ cm^2 s^{-1}, $D_E = 4 \times 10^{-9}$ cm^2 s^{-1}, $E_s = 0$, $K_M = 1$ μM, $k_2 = 10^3$ s^{-1}, $k_3 = 3000$ M^{-1} s^{-1}, $k_4 = 10^9$ M^{-1}s^{-1}, and $\omega = 3000$ rpm.

D_Z by fitting the i_L vs ln ω plot, recorded at a substrate concentration close to K_M (see Figure 7d). This procedure is then repeated until consistent values of D_Z and K_M are attained in two successive iterations.

(c.3) Kinetic Analysis in the Presence of Substrate Concentration Gradients. To minimize the extent of undesirable enzyme deactivation or inhibition processes, it may be necessary to carry out the kinetic analysis in the presence of low substrate concentrations. Under these circumstances, mass transport polarization cannot be avoided, and the kinetic analysis requires a more elaborate procedure.

First, the initial slopes Φ in the i_L vs c_Z^b plots are determined as a function of the electrode rotation rate, to give the values of $K_M/k_2\Gamma_E^T$ and Λ. Then, c_Z^s in eq AI.13 is expressed in terms of the catalytic current (i.e., $c_Z^s = c_Z^b - i_{cat}/2FA\Lambda$, see eq AI.14) and, after some rearrangement, it follows that:

$$\left(\frac{1}{|i_{cat}|} - \frac{1}{\Phi\, c_Z^b}\right)\left(1 - \frac{|i_{cat}|}{2FA\Lambda c_Z^b}\right)^{-1} = \frac{1+\xi}{2FAk_3^{ap}\Gamma_{OR}^T\Gamma_E^T} + \frac{1}{2FAk_2\Gamma_E^T} \quad (22)$$

so that a plot of the left-hand side against $1 + \xi$ provides the values of $k_3^{ap}\Gamma_{OR}^T\Gamma_E^T$ and $k_2\Gamma_E^T$. In the absence of mass transport control $|i_{cat}| \ll \Phi c_Z^b$ and $|i_{cat}| \ll 2FA\Lambda c_Z^b$, and the primary plot of Savéant et al.[20] is recovered. It should be noted that application of eq 22 is restricted to the $0.1 \leq |i_{cat}/i_L| \leq 0.9$ range, and requires a high experimental accuracy.

(d) Thin Layer Voltammetry of 3D Films. This type of kinetic analysis can also be applied to 3D catalytic films under the uniform thin layer conditions indicated previously, i.e., as far as the voltammetric response is not determined by the rates of electron hopping or substrate diffusion within the film. Usually, electron hopping is slower than substrate diffusion, and a case diagram for the applicability of the uniform thin layer model can be developed in terms of the following dimensionless parameters:

$$\sigma_1 = \frac{L^2/D_E}{RT/vF} \quad (23)$$

$$\sigma_2 = \frac{L^2/D_E}{1/k_3^{ap}\Gamma_E^T} \quad (24)$$

where L^2/D_E is the characteristic time scale for the diffusion-like electron hopping process, RT/vF for the voltammetric

potential perturbation, and $1/k_3^{ap}\Gamma_E^T$ for the regeneration of the mediator oxidized form. The rectangular box in the lower-left corner of the case diagram in Figure 8 a corresponds to σ_1 and σ_2 values leading to less than 1% current deviation between voltammograms computed with and without allowance for finite hopping rate. The case diagram has been derived for the saturated kinetic regime, which requires high fluxes within the film, and represents the most demanding conditions for the applicability of the uniform thin layer model.

Comparison between the voltammetric shapes predicted by the uniform thin layer model and those computed from eq AII.15 shows that a finite rate of charge transport across the film has a 2-fold effect on the voltammograms. If mediation kinetics are fast enough, so that $\ln \sigma_2 > -1.5$ (upper left corner in Figure 8a), the catalytic wave is shifted toward E_s, and if the scan rate is high enough, so that $\ln \sigma_1 > -0.4$ (lower right corner in Figure 8a), the surface redox component adopts the typical shape associated with diffusion control. As illustrated in Figure 8b, whenever electron hopping limits the rate of the catalytic cycle, either because the film is too thick (curves 1 and 4) or because the scan rate is too high (curves 1′ and 2′), the catalytic component of the current, obtained from $i_{cat} = i - i_{rdx}$, displays a hysteresis loop, characterized by higher currents in the backward than in the forward scan. Therefore, the uniform thin layer model applies only when the forward and backward redox subtracted traces coincide.

(e) Characterization of the Electrocatalytic Cycle for H_2O_2 Reduction by Immobilized Horseradish-Peroxidase. The previous theoretical treatment is now applied to the analysis of the electrocatalytic behavior of taurine-modified horseradish peroxidase (HRP) entrapped in a polyvinil pyridine−$[Os(bpy)_2Cl]^{2+/+}$ redox polymer. This system has been selected because it displays an efficient electrical connection between enzyme and redox mediator, and because its unsaturated kinetic region appears at very low substrate concentrations, illustrating the importance of the mass transport effects in the kinetic analysis.

According to previous results in solution,[21] the basic peroxidase catalytic cycle for immobilized HRP can be formulated as follows:

$$HRP\ (ER) + H_2O_2\ (Z) \underset{k_{-1}}{\overset{k_1}{\rightleftharpoons}} HRP{\cdot}H_2O_2\ (EZ) \qquad (25)$$

$$HRP{\cdot}H_2O_2\ (EZ) \xrightarrow{k_2} HRP\text{-}I\ (EO) + H_2O\ (P) \qquad (26)$$

$$HRP\text{-}I\ (EO) + R \xrightarrow{k_3} HRP\text{-}II\ (EO') + O \qquad (27)$$

$$HRP\text{-}II\ (EO') + R \xrightarrow{k_4} HRP\ (ER) + O \qquad (28)$$

where R and O stand for $[Os(bpy)_2Cl]^+$ and $[Os(bpy)_2Cl]^{2+}$, respectively, HRP represents the native ferriperoxidase, HRP·H_2O_2 is the precursor complex, HRP-I is the oxidized form of the enzyme containing an oxyferryl group (Fe^{IV}=O) and a π−cation radical in the porphyrin ring, and HRP-II is an intermediate oxidized state of the enzyme obtained from the reduction of the π−cation radical by cosubstrate R. Although the reaction of HRP with H_2O_2 has often been described as an irreversible bimolecular step, there exists evidence for the formation of a precursor complex between HRP and H_2O_2, prior to the generation of compound HRP-I.[22]

At high H_2O_2 concentrations, the above mechanism is complicated by two additional pathways, leading to the inactivation of the enzyme. A first inactivation route implies the irreversible conversion of compound I into a verdohaemoprotein (P670), which represents a dead end in the catalytic cycle.[23] The second route involves the formation of oxyperoxidase (commonly known as compound III), which can be converted back to either the native HRP, by spontaneous decomposition, or to HRP-I, by reaction with a reducing substrate such as the actual redox mediator.[24] Recently, a detailed mechanistic study of these processes in solution has been reported by Dequaire et al.[24d] Here we focus on a similar system, having both enzyme and cosubstrate immobilized on the electrode surface, and perform our study under conditions where inactivation is negligible. Preliminary experiments showed that, for typical H_2O_2 concentration values in the saturated kinetic region (i.e., 600−800 μM), it takes ca. 15 min for the amperometric current to decay 5% of its initial value, this time interval being long enough to record the voltammetric response of a given enzyme electrode without significant deactivation.

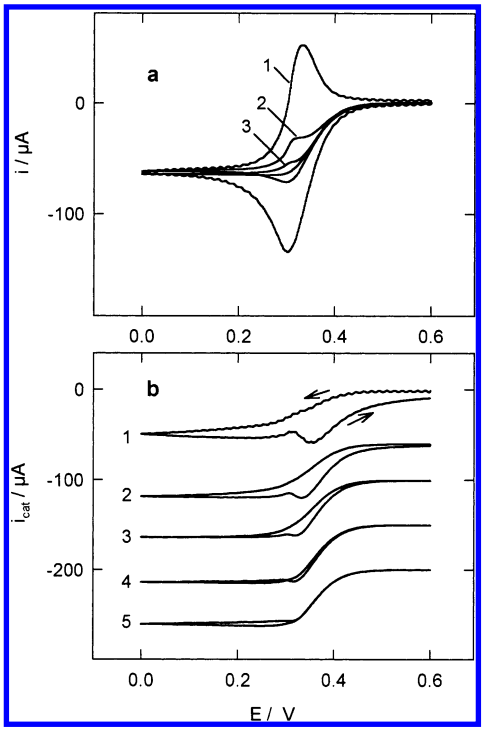

Figure 9. (a) Voltammetric response of the HRP−Os modified electrode in the presence of a 416 μM H_2O_2 solution, as a function of the potential scan rate v/mV s^{-1}: (1) 50, (2) 10, (3) 3. (b) Catalytic currents obtained after subtraction of the redox component from the observed currents in part a, including also the response for (4) 1 mV s^{-1} and (5) 0.5 mV s^{-1}. Electrode rotation rate ω = 3200 rpm

As discussed previously, the applicability of the uniform thin layer model to 3D biosensor structures is limited to low enough scan rates, where electron hopping does not limit the rate of charge transport across the film. To determine the maximum allowable scan rate, a series of voltammograms were recorded as a function of scan rate, and they are reproduced in Figure 9a. When the current due to the redox conversion of the osmium centers is subtracted from these voltammograms (Figure 9b), it may be observed that the onset of significant hysteresis takes place within the 5−10 mV s^{-1} scan rate interval, leading to 3.4 s $\geq L^2/D_E \geq$ 1.7 s, according to the case diagram depicted in Figure 8a. The thickness of the enzyme electrodes can be estimated from the surface concentration of redox centers $\Gamma_{OR}^T = 3.9 \times 10^{-8}$ mol cm^{-2}, by assuming a volume concentration value $\Gamma_{OR}^T/L \approx 4.7 \times 10^{-4}$ mol cm^{-3} as reported in the literature,[6b] to obtain $L \approx 0.8$ μm. When this thickness value is combined with the L^2/D_E ratio given above, a value of $D_E = 2.6 \pm 0.5 \times 10^{-9}$ cm^2 s^{-1} is obtained, which is consistent with

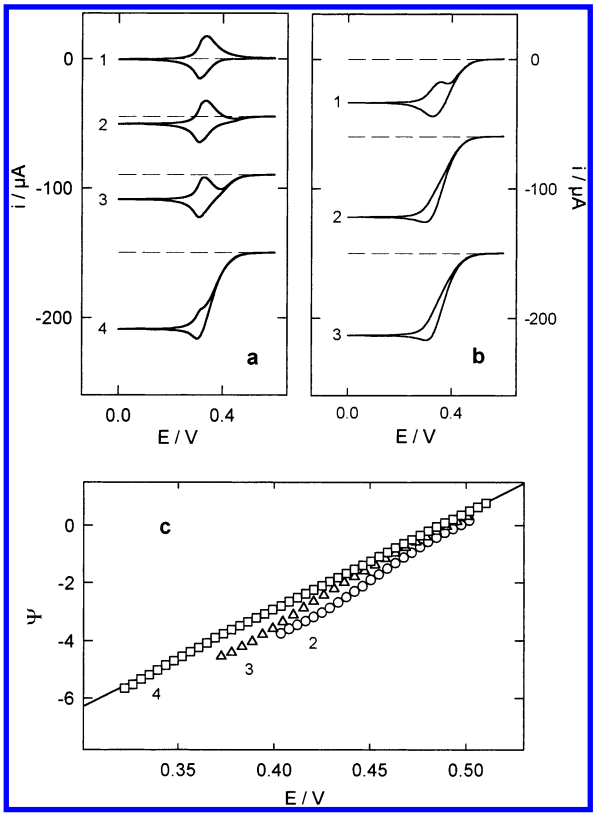

Figure 10. (a) Influence of H_2O_2 concentration on the voltammetric shapes. $c^b_{H_2O_2}/\mu$M:(1) 0, (2) 20, (3) 90, and (4) 600. Voltammograms have been shifted vertically for clarity. Other parameter values: $\upsilon = 3$ mV s^{-1} and $\omega = 1500$ rpm (b) Influence of electrode rotation rate on the voltammetric shapes. ω/rpm: (1) 100, (2) 1500, and (3) 3200. Voltammograms have been shifted vertically for clarity. Other parameter values: $\upsilon = 3$ mV s^{-1} and $c^b_{H_2O_2} = 400$ μM. (c) Test for the validity of the $c^b_{H_2O_2} \approx c^s_{H_2O_2}$ approximation (see eq 22) along voltammograms 2−4 in part a.

previous D_E estimates ($2-4 \times 10^{-9}$ cm^2/s) for this particular polymer.[6a] Therefore, a scan rate of 3 mV s^{-1} was selected for the present study, to keep the electrochemical response of the redox polymer close to nernstian conditions and to minimize the extent of enzyme deactivation.

In the absence of substrate in solution, bell shaped voltammograms, typical of a surface confined redox process, are recorded (see Figure 10a). The difference between anodic and cathodic peak potentials ΔE is ca. 25 mV, and it remains scan rate independent for $\upsilon \leq 50$ mVs^{-1}, suggesting that this peak difference is not due to a kinetically controlled process. The average of the two peak potentials gives $E_s = 0.333$ V for the mediator redox couple.

Upon increasing the substrate concentration in solution, a sigmoidal catalytic current develops at potentials more positive than E_s, and eventually, the catalytic wave shifts slightly toward more negative potentials, indicating that a greater amount of reduced osmium centers are required to restore the native state of the enzyme. The analysis of the Ψ vs E plots in Figure 10c shows that, for $\omega = 1500$ rpm, mass transport effects can be neglected at the higher H_2O_2 concentrations (≥ 600 μM) only. This conclusion is further supported by the influence of the electrode rotation speed on the catalytic current shown in Figure 10b. The slope of the linear Ψ vs E plots was found to be scan rate independent for $\upsilon \leq 3$ mV s^{-1} and equal to $0.9F/RT$, i.e., somewhat smaller than expected for ideal nernstian behavior of the redox polymer and in agreement with similar findings in related systems.[6c,d]

Figure 11, parts a and b, illustrate the variation of $E_{1/2}$ and i_L with H_2O_2 concentration in solution. By inserting the $c^b_{H_2O_2} \rightarrow \infty$ limiting values of the catalytic current $i_L^{sat} = -63$ μA and half-wave potential $E^{sat}_{1/2} = 0.357$ V in eqs 10 and 15−16, $k_3^{ap}\Gamma^T_{OR}/k_2 = 1.6$ and $k_2\Gamma^T_E = 2.7 \times 10^{-9}$ mol cm^{-2} s^{-1} were obtained. Because $k_3^{ap}\Gamma^T_{OR} > k_2$, it turns out that the conversion of the HRP−H_2O_2 complex to produce HRP-I and H_2O is the rate-limiting step of the biosensor response under saturation conditions. This observation agrees with the results obtained from the analysis of the HRP catalytic activity in homogeneous solution in the presence of rapidly oxidized *o*-diphenols.[22c] The pseudo-first-order rate constant $k_3^{ap}\Gamma^T_E = 0.11$ s^{-1} probably reflects the time-scale for the reduction of HRP-II (i.e., $k_3^{ap} \approx k_4$), because this step has been shown to be slower than the reduction of HRP-I.[22c,24d]

The initial slope Φ of the i_L vs $c^b_{H_2O_2}$ plots defines the sensitivity of the biosensor (see eq 21). Values of Φ have been found to increase from 0.48 A cm^{-2} M^{-1} at 100 rpm to 1.8 A cm^{-2} M^{-1} at 3200 rpm, and they are ca. 20% higher than the previous maximum value reported in the literature for polymer-based peroxidase biosensors.[25] According to eq 21, this improvement in sensitivity should be traced back to a higher $k_2\Gamma^T_E/K_M$ value when HRP modified with negatively charged taurine is used. Preliminary experiments in solution showed a decrease of ∼30% in the catalytic activity of HRP after modification, and therefore, the influence of taurine is most likely related to an increase in the number of enzyme molecules which are effectively wired to the redox polymer (see also below), because of a stronger electrostatic attraction between enzyme and polymer.

An initial estimate of the diffusion coefficient of H_2O_2 (∼1.4×10^{-5} cm^2 s^{-1}) and of the Michaelis constant (∼70 μM) was obtained from the electrode rotation rate dependence of the i_L vs $c^b_{H_2O_2}$ limiting slopes. Then, a more precise determination was made from the variation of the steady-state limiting current with the electrode rotation rate, under nearly saturated kinetic conditions (Figure 11c). By applying the optimization procedure described before (see section c.2), satisfactory fits of the i_L vs $c^b_{H_2O_2}$ and i_L vs ω plots to eq 4 were obtained with $D_{H_2O_2} = 1.5 \times 10^{-5}$ cm^2 s^{-1} and $K_M = 71$ μM (solid lines in Figure 11, parts a and b). The good agreement with the $D_{H_2O_2}$ estimate reported by Prabhu et al.[26] (1.6×10^{-5} cm^2 s^{-1}) and the satisfactory prediction of the $E_{1/2}$ dependence on $c^b_{H_2O_2}$ depicted in Figure 11b give additional support to the proposed kinetic analysis and indicate a facile diffusion transport of H_2O_2 throughout the film. Moreover, the K_M value is similar to those reported from experiments with different reducing cosubstrates in solution. For example, Baek et al.[22a] estimated a value of $K_M = 46$ μM, by extrapolating at 25 °C the results obtained with stopped-flow cryoenzymology at subzero temperatures. Rodriguez-López et al.[22c] obtained cosubstrate-dependent K_M values in the 27−128 μM range, by using a series of *o*-diphenols as electron donors. Also a value of 128 μM was used by Dequaire et al.[24d] to fit the electrocatalytic response of HRP in the presence of the reducing $[Os(bpy)_2pyCl]^+$ complex in solution.

It should be noted that the time scales of electron hopping through the polymer and mediation between enzyme and polymer are similar so that $\ln \sigma_2 = \ln(k_3^{ap}\Gamma^T_E/D_E/L^2) = -1.3$, which is a value close to the limit of applicability of the thin layer model (see Figure 8a). Therefore, it was decided to explore the influence of the electron hopping rate on our previous analysis. Equation AII.15 was solved numerically with $D_E = 2.6 \times 10^{-9}$ cm^2 s^{-1} and $L = 0.8$ μm, as indicated in Appendix

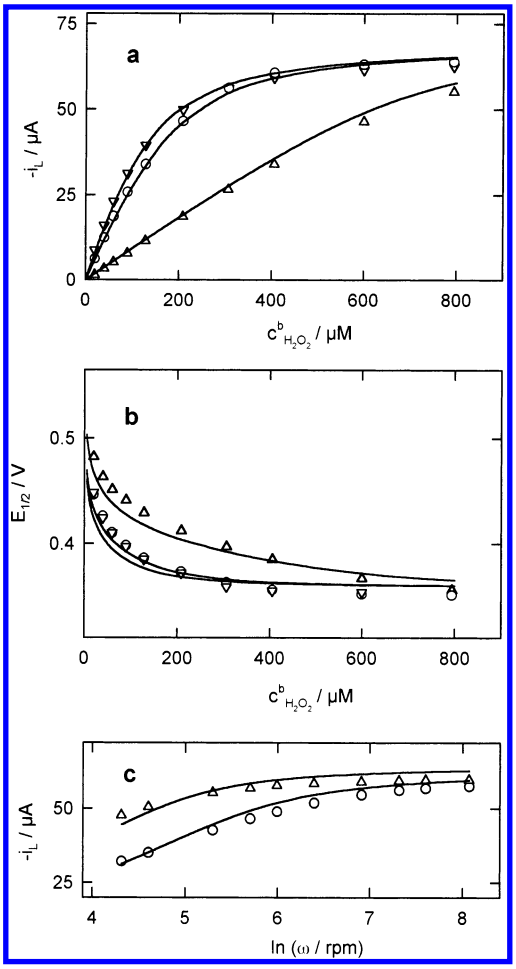

Figure 11. (a) Variation of the catalytic limiting current with H_2O_2 concentration, as a function of the electrode rotation rate ω/rpm (▽) 3200, (○) 1500, and (△) 100. (b) Variation of the catalytic half-wave potential with H_2O_2 concentration, as a function of the electrode rotation rate ω/rpm (▽) 3200, (○) 1500, and (△) 100. (c) Variation of the catalytic limiting current with electrode rotation rate, as a function of H_2O_2 concentration $c^b_{H_2O_2}/\mu$M: (○) 401 and (▽) 600. In all cases, solid lines are theoretical predictions corresponding to the values of the kinetic parameters indicated in the text.

II, and quantitative fits such as those shown in Figures 10−11 were obtained for $k_2\Gamma_E^T = 2.5 \times 10^{-9}$ mol cm^{-2} s^{-1}, $k_3^{ap}\Gamma_E^T = 0.16$ s^{-1}, $K_M = 71$ μM, and $D_{H_2O_2} = 1.5 \times 10^{-5}$ cm^2 s^{-1}. Thus, explicit consideration of the electron hopping rate produces a somewhat higher estimate of $k_3^{ap}\Gamma_E^T$ and barely modifies the $k_2\Gamma_E^T$ value derived from the uniform layer model. The small influence of electron hopping on the biosensor response is further illustrated by noting that the i_L^{sat} value would increase by less than 5% if the charge transport through the polymer were infinitely fast.

Under thin-layer electrochemical conditions, the kinetic behavior of the biosensor becomes fully determined, by specifying the values of $k_3^{ap}\Gamma_{OR}^T\Gamma_E^T$, $k_2\Gamma_E^T$, K_M, and $D_{H_2O_2}$. However, a comparison of the k_3^{ap} and k_2 values with the catalytic results of Dequaire et al.[24d] in homogeneous solution can be carried out by assuming that the surface concentration of active and electronically wired enzymes Γ_E^T coincides with the surface concentration of the deposited enzymes, i.e., $\Gamma_E^T = 2.9 \times 10^{-10}$ mol cm^{-2}. Then, from the previous $k_3^{ap}\Gamma_{OR}^T\Gamma_E^T$ and $k_2\Gamma_E^T$ values, and by inserting $L = 0.8$ μm in eq 14, one obtains $(k_3^{ap})_{hom} = 44$ M^{-1} s^{-1} and $k_2 = 9$ s^{-1}. This last value is ca. 200 times smaller than that reported by Dequaire et al.[24d] Comparison of $(k_3^{ap})_{hom}$ is not so straightforward, because these authors use a Michaelis−Menten formalism to model the mediation steps, but in the low cosubstrate concentration limit $(k_3^{ap})_{hom}$ becomes ca. 3×10^5 times smaller than its analogue obtained in homogeneous solution.[24d] As far as the immobilization process does not greatly affect the enzyme turnover number, this comparison suggests that only a small percentage (∼1%) of the immobilized enzymes participate in the charge transducing cycle and that an even smaller percentage of the electrically connected redox centers are directly involved in electron exchange with these enzymes (i.e., $\chi_R^{EO'} \sim 0.1\%$ in eq AI.5). It should be noted that Calvo et al.[6d,e] reached a similar conclusion in relation to the electrical wiring efficiency of supramolecular structures composed of alternate layers of negatively charged glucose oxidase and a cationic redox polyelectrolyte.

It follows from the previous discussion that the catalytic current generated by the Os−HRP modified electrode is mainly governed by the rate of enzyme oxidation. Charge transfer from the redox relays to the enzyme turns out to be quite efficient, and it takes place in a time scale similar to that of electron hopping through the polymer. This last process is shown to produce only a slight perturbation of the overall catalytic response, which is mainly translated into a ∼5 mV cathodic shift of the voltammetric wave. Comparison with kinetic parameters obtained in homogeneous solution suggests that a significant improvement of performance could be achieved by increasing the number of enzymes which are effectively involved in electron exchange with the polymer network.

Conclusions

Analytical expressions describing the voltammetric response of a reagentless mediated enzyme electrode operated under rotating disk conditions have been worked out, taking into account substrate depletion outside the catalytic film. It is demonstrated that this simple model can be applied either to two-dimensional films or to the more commonly encountered three-dimensional films, as far as the latter are operated under thin-layer electrochemical conditions. Case diagrams and diagnostic criteria have been developed to assess the experimental conditions under which the model can be employed.

Horseradish peroxidase entrapped in an osmium functionalized polyvinyl pyridine polymer exhibits the typical features expected for an efficient electrical connection between the iron porphyrin group and the osmium redox centers, as evidenced by the appearance of the catalytic wave prior to the redox polymer features. Taurine modification of HRP favors its electrostatic immobilization within the cationic polymer, and it seems to be responsible for a significant increase in the $k_2\Gamma_E^T/K_M$ value, leading to a biosensor sensitivity 20% higher than the maximum value reported in the literature for polymer-based peroxidase electrodes. The characteristic $k_3^{ap}\Gamma_{OR}^T\Gamma_E^T/k_2\Gamma_E^T$ ratio turns out to be bigger than one, showing that the overall rate is mainly limited by the conversion of the HRP−H_2O_2 precursor complex into the oxidized HRP-I form of the enzyme and not by any of the mediation steps. Determination of K_M under unsaturated kinetic conditions requires the consideration of H_2O_2 mass transport, and the value obtained (71 μM) lies within the range reported for homogeneous mediation (27−128 μM). The good agreement between the value obtained for the H_2O_2 diffusion coefficient and that quoted in the literature, from studies on a bare electrode surface, indicates an easy permeation of the substrate through the film. A comparison with kinetic

parameter values obtained by Dequaire et al.[24d] in homogeneous solution suggests that a significant improvement of the biosensor performance would be achieved by increasing the fraction of enzymes which are effectively connected to the redox polymer.

Acknowledgment. J. J. C. and R. A. acknowledge financial support from the DGICYT under Grant PB098-1123. A.N. and E.D. acknowledge financial support from the Spanish Ministry of Science and Technology (BIO 1999-1213). A.N. acknowledges a postdoctoral fellowship from the Community of Madrid. Helpful comments by Dr. W. H. Mulder are also gratefully acknowledged.

Appendix I

In this appendix, the rotating disk boundary value problem associated with the catalytic mechanism depicted in Figure 1a is described. Assuming a fast and reversible electron exchange between electrode and mediator (eq 1), the surface concentrations of the oxidized and reduced forms of the mediator depend on the applied potential E according to

$$\Gamma_O(E) = \frac{\Gamma_{OR}^T \xi}{1+\xi} \tag{AI.1}$$

$$\Gamma_R(E) = \frac{\Gamma_{OR}^T}{1+\xi} \tag{AI.2}$$

where $\Gamma_{OR}^T = \Gamma_O + \Gamma_R$ stands for the total surface concentration of mediator, and

$$\xi = \exp\left\{\frac{F}{RT}(E - E_s)\right\} \tag{AI.3}$$

It should be noted that only a fraction of the mediator centers are in direct contact with the enzymes and, therefore, can participate in the enzyme-mediator electronic exchange. Because this fraction is usually unknown, it is convenient to define the second-order rate constants k_3^s and k_4^s for the mediation steps as follows:

$$\upsilon_{2a} = k_3^* \chi_R^{EO} \Gamma_R \Gamma_{EO} = k_3^s \Gamma_R \Gamma_{EO} \tag{AI.4}$$

$$\upsilon_{2b} = k_4^* \chi_R^{EO'} \Gamma_R \Gamma_{EO'} = k_4^s \Gamma_R \Gamma_{EO'} \tag{AI.5}$$

where v_{2a} and v_{2b} are the rates of steps 2a and 2b, Γ_{EO} and $\Gamma_{EO'}$ are the surface concentrations of the two oxidized forms of the enzyme, and χ_R^{EO} and $\chi_R^{EO'}$ are the fractions of Γ_R that are involved in electron exchange with EO and EO′, respectively.

By adopting the steady-state hypothesis for the intermediate forms of the enzyme, i.e., by setting all $d\Gamma_{Ei}/dt$ derivatives equal to zero in the reaction scheme described by eqs 1−3, their surface concentrations can be expressed as follows:

$$\Gamma_{EO} = \frac{\Gamma_E^T}{\Omega^s} \tag{AI.6}$$

$$\Gamma_{EZ} = \frac{k_3^s \Gamma_{OR}^T \Gamma_E^T}{k_2 (1+\xi) \Omega^s} \tag{AI.7}$$

$$\Gamma_{ER} = \frac{k_3^s K_M \Gamma_{OR}^T \Gamma_E^T}{k_2 (1+\xi) c_Z^s \Omega^s} \tag{AI.8}$$

$$\Gamma_{EO'} = \frac{k_3^s \Gamma_E^T}{k_4^s \Omega^s} \tag{AI.9}$$

where $\Gamma_E^T = \Gamma_{EO} + \Gamma_{EZ} + \Gamma_{ER} + \Gamma_{EO}$ is the total surface concentration of enzyme, c_Z^s is the substrate concentration at the electrode surface, and K_M (the enzyme−substrate Michaelis constant) and Ω^s are defined as

$$K_M = \frac{k_{-1} + k_2}{k_1} \tag{AI.10}$$

$$\Omega^s = 1 + \frac{k_3^s}{k_4^s} + \frac{k_3^s \Gamma_{OR}^T}{k_2 (1+\xi)} \left(1 + \frac{K_M}{c_Z^s}\right) \tag{AI.11}$$

According to the steady-state hypothesis, the catalytic current is given by

$$i_{cat} = -2FAk_3^s \Gamma_{EO} \Gamma_R \tag{AI.12}$$

where F is the Faraday constant and A is the electrode surface area. By substituting eqs AI.2 and AI.6 into eq AI.12 and rearranging, it follows that

$$-\frac{2FA}{i_{cat}} = \left(\frac{1}{k_3^s} + \frac{1}{k_4^s}\right) \frac{1+\xi}{\Gamma_{OR}^T \Gamma_E^T} + \frac{1}{k_2 \Gamma_E^T} \left(1 + \frac{K_M}{c_Z^s}\right) \tag{AI.13}$$

which shows clearly how the catalytic current results from a series connection of a potential dependent mediation step (first term on the right-hand side) and a potential independent enzymatic step (second term on the right-hand side). It may also be noted that the externally applied potential determines the number of active mediator centers ($\Gamma_{OR}^T/(1+\xi)$), whereas the electrode rotation acts on the substrate concentration at the enzymatic layer (c_Z^s).

An explicit expression for c_Z^s can be obtained from the flux balance of substrate at the electrode surface

$$j_Z = D_Z \left(\frac{\partial c_Z}{\partial x}\right)_{x=0} = -\Lambda (c_Z^s - c_Z^b) = k_1 c_Z^s \Gamma_{ER} - k_{-1} \Gamma_{EZ} \tag{AI.14}$$

where D_Z is the substrate diffusion coefficient, c_Z^b is the substrate concentration in the bulk of the solution, and Λ is the mass transport coefficient, defined as[19]

$$\Lambda = 0.62 \nu^{-1/6} D_Z^{2/3} \omega^{1/2} \tag{AI.15}$$

where ν and ω are the kinematic viscosity of the solution and the electrode rotation rate, respectively. Then, it follows from eq AI.14 that

$$c_Z^s = \frac{\Lambda c_Z^b + k_{-1} \Gamma_{EZ}}{\Lambda + k_1 \Gamma_{ER}} \tag{AI.16}$$

By combining eq AI.16 with eqs AI.6−AI.9, the following expressions for the different forms of the enzyme are obtained:

$$\Gamma_{EO} = \frac{2B_0 \Gamma_E^T}{H + \sqrt{H^2 - 4G}} \tag{AI.17}$$

TABLE 1: Definition of the B_i, H, G, and U Kinetic Parameters

$$B_0 = \frac{k_4^s}{k_3^s + k_4^s} \qquad B_1 = \frac{k_3^{ap}\,\Gamma_{OR}^T}{k_2\,(1+\xi)} \qquad B_2 = \frac{K_M\,k_3^{ap}\,\Gamma_{OR}^T}{k_2\,c_Z^b\,(1+\xi)}$$

$$H = 1 + \frac{k_3^{ap}\Gamma_{OR}^T}{k_2(1+\xi)}\left\{1 + \frac{K_M}{c_Z^b} + \frac{k_2\Gamma_E^T}{\Lambda c_Z^b}\right\} \qquad G = \frac{k_3^{ap}\Gamma_E^T\Gamma_{OR}^T}{\Lambda c_Z^b(1+\xi)}\left(1 + \frac{k_3^{ap}\Gamma_{OR}^T}{k_2(1+\xi)}\right) \qquad U = \frac{k_3^{ap}\Gamma_E^T\Gamma_{OR}^T}{\Lambda c_Z^b(1+\xi)}$$

$$\Gamma_{EZ} = \frac{2B_1\Gamma_E^T}{H + \sqrt{H^2 - 4G}} \tag{AI.18}$$

$$\Gamma_{ER} = \frac{2B_2\Gamma_E^T}{H + \sqrt{H^2 - 4G} - 2U} \tag{AI.19}$$

$$\Gamma_{EO'} = \frac{2(1 - B_0)\Gamma_E^T}{H + \sqrt{H^2 - 4G}} \tag{AI.20}$$

where the kinetic parameters H, G, U, B_0, B_1, and B_2 are defined in Table 1 in terms of an overall rate constant for redox mediation k_3^{ap}

$$k_3^{ap} = \frac{k_3^s k_4^s}{k_3^s + k_4^s} \tag{AI.21}$$

It should be pointed out that the use of k_3^{ap}, incorporating the values of both k_3^s and k_4^s, reduces the actual catalytic cycle to an apparent single redox-enzyme cycle. The value of k_3^{ap} is a direct measure of the rate of electron transfer between enzyme and mediator, and its optimization plays a central role in the design of this type of biosensors.

When the voltammetric scan rate υ is kept low enough (typically, <0.5 V s^{-1}), nonfaradaic contributions to the observed current i can be neglected, which can be assumed to consist of two contributions. One contribution (i_{rdx}) originates in the change of the mediator redox state, and the second contribution (i_{cat}) results from the catalytic conversion of the substrate

$$i = i_{rdx} + i_{cat} = FA\left(\upsilon\frac{d\Gamma_O}{dE} - 2k_3^s\Gamma_{EO}\Gamma_R\right) \tag{AI.22}$$

where transient contributions from any of the enzymatic forms have been neglected. By differentiating eq AI.1 with respect to the potential and substituting eqs AI.2 and AI.17 into eq AI.22, the following expression is obtained:

$$i = \frac{FA\Gamma_{OR}^T}{1+\xi}\left(\mp\frac{\upsilon F}{RT}\frac{\xi}{1+\xi} - \frac{4k_3^{ap}\,\Gamma_E^T}{H + \sqrt{H^2 - 4G}}\right) \tag{AI.23}$$

where the minus sign preceding the first term within brackets applies to the negative-going scan, and the plus sign to the positive-going scan.

Appendix II

In this appendix, the rotating disk boundary value problem associated with the catalytic mechanism depicted in Figure 1c is described. Under conditions where diffusion of the enzyme and of the redox mediator within the film are negligible, their total concentrations c_E^T and c_{OR}^T remain time and position independent, and the following identities hold:

$$c_{OR}^T = c_R(x,t) + c_O(x,t) \tag{AII.1}$$

$$c_E^T = c_{ER}(x,t) + c_{EO}(x,t) + c_{EZ}(x,t) + c_{EO'}(x,t) \tag{AII.2}$$

A minimum of five mass balance differential equations is required to obtain the voltammetric response associated with the catalytic mechanism. These are the following:

$$\frac{\partial c_O}{\partial t} = D_E\frac{\partial^2 c_O}{\partial x^2} + k_3 c_R c_{EO} + k_4 c_R c_{EO'} \tag{AII.3}$$

$$\frac{\partial c_Z}{\partial t} = D_Z\frac{\partial^2 c_Z}{\partial x^2} - k_1 c_Z c_{ER} + k_{-1} c_{EZ} \tag{AII.4}$$

$$\frac{\partial c_{EZ}}{\partial t} = k_1 c_Z c_{ER} - (k_{-1} + k_2)c_{EZ} \tag{AII.5}$$

$$\frac{\partial c_{EO}}{\partial t} = k_2 c_{EZ} - k_3 c_{EO} c_R \tag{AII.6}$$

$$\frac{\partial c_{EO'}}{\partial t} = k_3 c_{EO} c_R - k_4 c_{EO'} c_R \tag{AII.7}$$

where the first term on the right-hand side of eq AII.3 stands for the diffusion-like electron hopping process, D_E being its apparent diffusion coefficient, D_Z is the substrate diffusion coefficient, which is assumed to be the same inside and outside the film, and k_3 and k_4 include the fraction of c_R involved in electron exchange with the oxidized forms of the enzyme, as stated in eqs AI.4 and AI.5 in Appendix I.

The definition of the boundary value problem is completed with the following initial conditions:

$$c_O(x,0) = \frac{c_{OR}^T\xi}{1+\xi} \tag{AII.8}$$

$$c_Z(x,0) = c_Z^b \tag{AII.9}$$

$$c_{EO}(x,0) = c_E^T;\ c_{ER}(x,0) = c_{EZ}(x,0) = c_{EO'}(x,0) = 0 \tag{AII.10}$$

and boundary conditions

$x = 0$:

$$c_O(0,t) = \frac{c_{OR}^T \xi}{1+\xi} \quad \text{(AII.11)}$$

$$D_Z\left(\frac{\partial c_Z}{\partial x}\right)_{x=0} = 0 \quad \text{(AII.12)}$$

$x = L$:

$$D_E\left(\frac{\partial c_O}{\partial x}\right)_{x=L} = 0 \quad \text{(AII.13)}$$

$$D_Z\left(\frac{\partial c_Z}{\partial x}\right)_{x=L} = -\Lambda(c_Z(L,t) - c_Z^b) \quad \text{(AII.14)}$$

where c_Z^b is the bulk concentration of substrate, ξ is the Nernst factor defined in eq AI.3, and Λ is the mass transport coefficient defined in eq AI.15 in Appendix I.

The voltammetric current is then computed from the concentration gradient of oxidized mediator at the electrode surface

$$i = -nFAD_E\left(\frac{\partial c_O}{\partial x}\right)_{x=0} \quad \text{(AII.15)}$$

A reasonable approximation in solving cyclic catalytic mechanisms is to assume steady-state conditions for each form of the enzyme. By imposing the $\partial c_i/\partial t = 0$ condition in eqs AII.5−AII.7 and combining them with eq AII.2, the following expressions are obtained for the partitioning of the enzyme into its different forms:

$$c_{EO} = \frac{c_E^T}{\Omega} \quad \text{(AII.16)}$$

$$c_{EZ} = \frac{k_3 c_R c_E^T}{k_2 \Omega} \quad \text{(AII.17)}$$

$$c_{ER} = \frac{k_3 K_M c_R c_E^T}{k_2 c_Z \Omega} \quad \text{(AII.18)}$$

$$c_{EO'} = \frac{k_3 c_E^T}{k_4 \Omega} \quad \text{(AII.19)}$$

where the potential and distance dependent parameter Ω is defined as

$$\Omega = 1 + \frac{k_3}{k_4} + \frac{k_3 c_R}{k_2}\left(1 + \frac{K_M}{c_Z}\right) \quad \text{(AII.20)}$$

and K_M is the Michaelis constant.

Under the above restrictions, the boundary value problem is reduced to two partial differential equations

$$\frac{\partial c_O}{\partial t} = D_E \frac{\partial^2 c_O}{\partial x^2} + \frac{2k_3 c_R c_E^T}{\Omega} \quad \text{(AII.21)}$$

$$\frac{\partial c_Z}{\partial t} = D_Z \frac{\partial^2 c_Z}{\partial x^2} - \frac{k_3 c_R c_E^T}{\Omega} \quad \text{(AII.22)}$$

which are subject to the initial and boundary conditions AII.8, AII.9, and AII.11−AII.14. The expression for c_R, is supplied by eq AII.1. In this work, eqs AII.21 and AII.22 are solved numerically by using the spline version of the orthogonal collocation technique, as described previously.[27] This numerical solution is mainly used for establishing the conditions where the analytical expressions derived for the 2D model can be applied to describe the voltammetric response of a 3D catalytic film.

References and Notes

(1) (a) Turner, A. P. F.; Karube, I.; Wilson, G. S. *Biosensors, Fundamentals and Applications*; Oxford University Press: Oxford, 1987. (b) Heller, A. *Acc. Chem. Res.* **1990**, *23*, 128. (c) Blum, L. J.; Coulet, P. R. *Biosensors, Principles and Applications*; Marcel Dekker: New York, 1991. (d) Bourdillon, C.; Demaille, C.; Moiroux, J.; Savéant, J. M. *Acc. Chem. Res.* **1996**, *29*, 529. (e) Willner, I.; Katz, E.; Willner, B. *Electroanalysis* **1997**, *9*, 965. (f) Willner, I.; Katz, E. *Angew. Chem., Int. Ed.* **2000**, *39*, 1180.

(2) (a) Armstrong, F. A.; Hill, H. A. O.; Walton, N. J. *Acc. Chem. Res.* **1988**, *21*, 407. (b) McLendon, G. *Acc. Chem. Res.* **1988**, *21*, 160. (c) Armstrong, F. A.; Wilson, G. S. *Electrochim. Acta* **2000**, *45*, 2623.

(3) Vreeke, M.; Maidan, R.; Heller, A. *Anal. Chem.* **1992**, *64*, 3084.

(4) (a) Degani, Y.; Heller, A. *J. Phys. Chem.* **1987**, *91*, 1285. (b) Degani, Y.; Heller, A. *J. Am. Chem. Soc.* **1988**, *110*, 2615. (c) Willner, I.; Katz, E.; Lapidot, N.; Bäuerle, P. *Bioelectrochem. Bioenerg.* **1992**, *29*, 29. (d) Schuhmann, W. *Biosens. Bioelectron.* **1995**, *10*, 181. (e) Willner, I.; Katz, E.; Riklin, A.; Kasher, R. *J. Am. Chem. Soc.* **1992**, *114*, 10965. (f) Willner, I.; Lapidot, N.; Riklin, A.; Kasher, R.; Zahavy, E.; Katz, E. *J. Am. Chem. Soc.* **1994**, *116*, 1428.

(5) (a) Kajiya, Y.; Okamoto, T.; Yoneyama, H. *Chem. Lett.* **1993**, 2107. (b) Rubin, S.; Chow, J. T.; Ferraris, J. P.; Zawodzinski, T. A. *Langmuir* **1996**, *12*, 363. (c) Bardea, A.; Katz, E.; Bückmann, A. F.; Willner, I. *J. Am. Chem. Soc.* **1997**, *119*, 9114. (d) Anicet, N.; Anne, A.; Moiroux, J.; Savéant, J. M. *J. Am. Chem. Soc.* **1998**, *120*, 7115. (e) Katz, E.; Heleg-Shabtai, V.; Willner, I.; Rau, H. K.; Haehnel, W. *Angew. Chem., Int. Ed. Engl.* **1998**, *37*, 3253. (f) Ruan, C.; Yang, F.; Lei, C.; Deng, J. *Anal. Chem.* **1998**, *70*, 1721. (g) Anicet, N.; Anne, A.; Bourdillon, C.; Demaille, C.; Moiroux J.; Savéant, J. M. *Faraday Discuss.* **2000**, *116*, 269.

(6) (a) Gregg, B. A.; Heller, A. *J. Phys. Chem.* **1991**, *95*, 5970. (b) Gregg, B. A.; Heller, A. *J. Phys. Chem.* **1991**, *95*, 5976. (c) Heller, A. *J. Phys. Chem.* **1992**, *96*, 3579. (d) Hodak, J.; Etchenique, R.; Calvo, E. J.; Singhal, K.; Bartlett, P. N. *Langmuir* **1997**, *13*, 2708. (e) Calvo, E. J.; Battaglini, F.; Danilowicz, C.; Wolosiuk, A.; Otero, M. *Faraday Discuss.* **2000**, *116*, 47. (f) Narvaez, A.; Suarez, G.; Popescu, I. C.; Katakis, I.; Dominguez, E. *Biosens. Bioelectron.* **2000**, *15*, 43.

(7) (a) Foulds, N. C.; Love, C. R. *J. Chem. Soc., Faraday Trans.* **1986**, *82*, 1259. (b) Bartlett, P. N.; Whitaker, R. G. *J. Electroanal. Chem.* **1987**, *224*, 37. (c) Bartlett, P. N.; Tebbutt, P.; Tyrrell, C. H. *Anal. Chem.* **1992**, *64*, 138. (d) Tatsuma, T.; Gondaira, M.; Watanabe, T. *Anal. Chem.* **1992**, *64*, 1183. (e) Palmisano, F.; Zamboni, P. G.; Centonze, D. *Fresenius J. Anal. Chem.* **2000**, *366*, 586. (f) Bartlett, P. N.; Cooper, J. M. *J. Electroanal. Chem.* **1993**, *362*, 1.

(8) Iwuoha, E. I.; Leister, I.; Miland, E.; Smyth, M. R.; Fágáin, C. *Anal. Chem.* **1997**, *69*, 1674. Iwuoha, E. I.; Smyth, M. R.; Lyons, M. E. G. *Biosens. Bioelectron.* **1997**, *12*, 53.

(9) (a) Bartlett, P. N.; Whitaker, R. G. *J. Electroanal. Chem.* **1987**, *224*, 27. (b) Bartlett, P. N.; Tebbutt, P.; Whitaker, R. G. *Prog. React. Kinet.* **1991**, *16*, 55.

(10) Bartlett, P. N.; Pratt, K. F. E. *Biosens. Bioelectron.* **1993**, *8*, 451.

(11) (a) Bergel, A.; Comtat, M. *Anal. Chem.* **1984**, *56*, 2904. (b) Lucisano, J. K.; Gough, D. A. *Anal. Chem.* **1988**, *60*, 1272. (c) Battaglini, F.; Calvo, E. J. *Anal. Chim. Acta* **1992**, *258*, 151. (d) Tatsuma, T.; Watanabe, T.; Okawa, Y. *Anal. Chem.* **1992**, *64*, 630. (e) Martens, N.; Hall, E. A. H. *Anal. Chem.* **1994**, *66*, 2763. (f) Yokoyama, K.; Kayanuma, Y. *Anal. Chem.* **1998**, *70*, 3368.

(12) (a) Brady, J. E.; Carr, P. W. *Anal. Chem.* **1980**, *52*, 977. (b) Leypoldt, J. K.; Gough, D. A. *Anal. Chem.* **1984**, *56*, 2896. (c) Gough, D. A.; Lucisano, J. Y.; Tse, P. H. S. *Anal. Chem.* **1985**, *57*, 2351. (d) Tse, P. H. S.; Gough, D. A. *Anal. Chem.* **1987**, *59*, 2339.

(13) (a) Andrieux, C. P.; Dumas-Bouchiat, J. M.; Savéant, J. M. *J. Electroanal. Chem.* **1982**, *131*, 1. (b) Leddy, J.; Bard, A. J.; Maloy, J. T.; Savéant, J. M. *J. Electroanal. Chem.* **1985**, *187*, 205. (c) Andrieux, C. P.; Savéant, J. M. In *Molecular Design of Electrode Surfaces*; Murray, R. W., Ed.; Techniques in Chemistry Series, Vol. 22; Wiley: New York, 1992.

(14) Albery, W. J.; Hillman, A. R. *J. Electroanal. Chem.* **1984**, *170*, 27.

(15) (a) Kulys, J. J.; Sorochinslii, V. V.; Vidziunaite, R. A. *Biosensors* **1986**, *2*, 135. (b) Bartlett, P. N.; Whitaker, R. G. *J. Electroanal. Chem.* **1987**, *224*, 27.

(16) (a) Bartlett, P. N.; Pratt, K. F. E. *J. Electroanal. Chem.* **1995**, *397*, 61. (b) Lyons, M. E. G.; Greer, J. C.; Fitzgerald, C. A.; Bannon, T.; Bartlett, P. N. *Analyst* **1996**, *121*, 715.

(17) Limoges, B.; Moiroux, J.; Savéant, J. M. *J. Electroanal. Chem.* **2002**, *521*, 8.

(18) Katakis, I.; Heller, A. *Anal. Chem.* **1992**, *64*, 1008.

(19) Bard, A. J.; Faulkner, L. R. *Electrochemical Methods. Fundamentals and Applications*; 2nd ed.; Wiley: New York, 2001; p 339.

(20) Bourdillon, C.; Demaille C.; Gueris, J.; Moiroux J.; Savéant, J. M. *J. Am. Chem. Soc.* **1993**, *115*, 12264.

(21) Dunford, H. B. *Heme Peroxidases*; Wiley: New York, 1999 and references therein.

(22) (a) Baek, H. K.; Van Wart, H. E. *Biochemistry* **1989**, *28*, 5714. (b) Baek, H. K.; Van Wart, H. E. *J. Am. Chem. Soc.* **1992**, *114*, 718. (c) Rodriguez-Lopez, J. N.; Gilabert, M. A.; Tudela, J.; Thorneley, R. N. F.; Garcia-Canovas, F. *Biochemistry* **2000**, *39*, 13201.

(23) (a) Nakajima, R.; Yamazaki, I. *J. Biol. Chem.* **1980**, *255*, 2067. (b) Rodriguez-Lopez, Hernandez-Ruiz, J.; Garcia-Canovas, F.; Thorneley, R. N. F.; Acosta, M.; Arnao, M. B. *J. Biol. Chem.* **1997**, *272*, 5469. (c) Hernadez-Ruiz, J.; Arnao, M. B.; Hiner, A. N. P.; Garcia-Canovas, F.; Acosta, M. *Biochem. J.* **2001**, *354*, 107.

(24) (a) Nakajima, R.; Yamazaki, I. *J. Biol. Chem.* **1987**, *262*, 2576. (b) Adediran, S. A.; Lambeir, A. M. *Eur. J. Biochem.* **1989**, *186*, 571. (c) Rodriguez-Lopez, J. N.; Smith, A. T.; Thorneley, R. N. F. *J. Biol. Chem.* **1997**, *272*, 389. (d) Dequaire, M.; Limoges, B.; Moiroux, J.; Savéant, J. M. *J. Am. Chem. Soc.* **2002**, *124*, 240.

(25) Ruzgas, T.; Csöregi, E.; Emnéus, J.; Gorton, L.; Marko-Varga, G. *Anal. Chim. Acta* **1996**, *330*, 123.

(26) Prabhu, V. G.; Zarapkar, L. R.; Dhaneshwar, R. G. *Electrochim. Acta* **1981**, *26*, 725.

(27) Calvente, J. J.; Andreu, R.; Gil, M. L. A.; González, L.; Alcudia, A.; Domínguez, M. *J. Electroanal. Chem.* **2000**, *432*, 18.